Article

A 1-Year Sediment Trap Study on the Downward Flux of Polycyclic Aromatic Hydrocarbons by Settling Particulate Matter in Deep Basins of the Aegean and Ionian Seas, Northeastern Mediterranean

Ester Skylaki [1,2,*], Constantine Parinos [1,*], Maria Tsagkaraki [2], Ioannis Hatzianestis [1], Anastasia Christidi [1], Elisavet Skampa [3], Ioanna Nikolopoulou [1,3], Georgia Kambouri [1], Ioanna Stavrakaki [1], Dimitris Velaoras [1], Giorgos Kouvarakis [2], Maria V. Triantaphyllou [3], Maria Kanakidou [2], Nikolaos Mihalopoulos [2,4] and Alexandra Gogou [1]

1   Institute of Oceanography, Hellenic Centre for Marine Research (HCMR), 46.7 km Athens-Sounion Av., 19013 Anavyssos, Greece; jhat@hcmr.gr (I.H.); anasch19@gmail.com (A.C.); nikolopoulou.ioa@gmail.com (I.N.); gkamb@hcmr.gr (G.K.); istavrakaki@hcmr.gr (I.S.); dvelaoras@hcmr.gr (D.V.); agogou@hcmr.gr (A.G.)
2   Environmental Chemical Processes Laboratory, Department of Chemistry, University of Crete, 71003 Heraklion, Greece; tsagaraki-maria@hotmail.com (M.T.); gkouvarakis@uoc.gr (G.K.); mariak@uoc.gr (M.K.); mihalo@uoc.gr (N.M.)
3   Faculty of Geology and Geoenvironment, National and Kapodistrian University of Athens, Panepistimioupolis, 15784 Athens, Greece; elskampa@geol.uoa.gr (E.S.); mtriant@geol.uoa.gr (M.V.T.)
4   Institute for Environmental Research and Sustainable Development, National Observatory of Athens, Lofos Koufou, P. Penteli, 15236 Athens, Greece
*   Correspondence: e.skylaki@hcmr.gr (E.S.); ksparinos@hcmr.gr (C.P.)

Abstract: This study investigates the composition, abundance, and vertical export of polycyclic aromatic hydrocarbons (PAHs) across three deep basins of the northeastern Mediterranean Sea (NEMS) over one year. Sinking particles were collected using sediment traps, and PAH analysis was conducted via gas chromatography-mass spectrometry. PAH fluxes varied significantly, peaking in the north Aegean Sea due to mesotrophic conditions, nutrient-rich riverine and Black Sea water inflows, and maritime anthropogenic inputs. The fluxes were highest in winter and lowest in fall. In the Cretan Sea, petrogenic sources (~70%) dominated, driven by currents, with fluxes highest in spring and lowest in winter. The Ionian Sea exhibited lower fluxes, peaking in summer and decreasing in fall. Atmospheric deposition seems to be the main transport pathway of pyrolytic PAHs in this site, while its high-water column depth (4300 m) compared to the other sites presumably enables extended degradation of organic constituents during particle settling. The positive matrix factorization (PMF) and principal component analysis (PCA) results reveal complementary insights into PAH sources and transport mechanisms. PMF analysis identified combustion (61%) and petrogenic (22%) sources, while PCA highlighted biogenic fluxes (57.7%) and atmospheric deposition. Seasonal productivity, riverine inputs, and water circulation shaped PAH variability, linking combustion-related PAHs to atmospheric soot and petrogenic PAHs to organic-rich particles.

Keywords: PAH; persistent organic pollutants; time series; settling particulate matter

1. Introduction

The oceans' ability to vertically transport and sequester sea surface-derived materials depends on a variety of biological and physiochemical processes, which mediate

particulate matter export from the surface to the deep ocean and eventually to marine sediments (known as the "biological pump") [1]. Due to the large variability observed on multiple spatial and temporal scales of the functioning of the biological pump, long-term observations are critical in order to allow the integration of the major mechanisms that are involved in the cycling of key chemical species/elements. Sediment traps, which allow the collection of space- and time-integrated sinking particulate matter as a result of the space- and time-dependency of the underlying processes, have proven valuable for biogeochemical studies in the world ocean [2–4].

Polycyclic aromatic hydrocarbons (PAHs) are a group of persistent organic pollutants (POPs) widely abundant in the marine environment. Several PAHs are known to have toxic, mutagenic, and/or carcinogenic properties [5], and 16 of them have been classified as priority pollutants by the U.S. Environmental Protection Agency (EPA-US), while 8 are prioritized by the European Union [6]. PAHs originate from human activities like the burning of biomass and fossil fuels, industrial processes, and petroleum-related activities [7]. Certain compounds, including retene and perylene, may originate from natural sources [8,9]. They reach the marine ecosystem via the atmosphere (dry/wet deposition, gas exchange at the air–water interface) and direct discharges, including oil spills, industrial outfalls, oil seepage, continental runoff, and rivers [10,11]. Owing to their hydrophobic nature, PAHs in marine settings are often adsorbed onto particles, leading to their subsequent transport to deeper ocean layers through settling particulate matter [12–15]. The structural properties of the different homologs largely determine their export potential and stability during their downward transport through the water column and final accumulation in marine sediments [16–18].

Up to date, few studies have provided time series data regarding the occurrence and export of PAHs in deep basins of the northeastern Mediterranean Sea (NEMS) [19,20]. Our study aims to identify major PAH sources, document the spatial and temporal variability of PAH concentrations and fluxes, and assess the main transport pathways and factors controlling their export to deep waters. However, a lack of knowledge still remains in regard to thoroughly investigating the control of the various components of the biological pump on their export and accumulation on a seasonal and annual scale. In this study, we report for the first time, to the best of our knowledge, a detailed evaluation of PAHs associated with sinking particles based on a 1-year sediment trap deployment in three deep basins of the NEMS. The marine areas under investigation include the north Aegean Sea, the south Aegean/Cretan Sea, and the Ionian Sea, areas with different characteristics, depths, and primary productivity. In addition, these areas are subjected to the influence of distinct mesoscale circulation features that largely determine their biogeochemical functioning and, consequently, PAH fate.

2. Oceanographic and Environmental Setting

The NEMS is considered as an ultra-oligotrophic region in terms of its biogeochemical features [21]. This oligotrophic regime is influenced by sub-basin gyres and mesoscale features, which alter water column biogeochemical properties through horizontal and vertical mass transfer. Carbon vertical flux varies along a north–south oligotrophy gradient, with net primary production (NPP) rates below $200 \, \text{mg C m}^{-2} \, \text{d}^{-1}$ and minimal organic carbon (<0.5% of NPP) reaching the deep-sea floor [22,23].

The NEMS is an area experiencing significant human-induced pressure, leading to the release of pollutants. The open NEMS, a significant area for commercial shipping and oil transit, has considerable petroleum emissions mostly along shipping routes (REMPEC MEDGIS-MAR) [24–26]. Moreover, the NEMS receives aerosols from polluted air masses from northern Europe and Saharan dust, rich in anthropogenic carbon-rich compounds

like black carbon. Over the course of a year, the north sector is dominant with almost 50% of the air masses reaching the NEMS originating from central and eastern Europe. During transition periods (spring/autumn), S/SW winds are responsible for Saharan dust transport (occurrence up to 20%) [27,28].

The marine areas under investigation in this study include the north Aegean Sea, the south Aegean/Cretan Sea, and the Ionian Sea (Figure 1). The north Aegean Sea is a marginal sea that connects the Black Sea to the NEMS through the Dardanelles Straits. Its biogeochemical functioning is largely determined by the interaction of the enriched in organic matter mesotrophic Black Sea Water (BSW) and the oligotrophic Levantine waters (LW) [29]. The differing physical properties of these two water masses cause the formation of a strong persistent thermohaline front in the area, impacting regional productivity [30]. During spring, the area shifts to a mesotrophic condition owing to increased BSW input, leading to enhanced primary production and planktonic biomass [31]. During winter, riverine-driven nutrient inputs also enhance productivity [32]. However, the average flow of the incoming BSW is estimated to be ~50-fold higher in comparison to freshwater inputs into the open northeastern Aegean Sea [33,34].
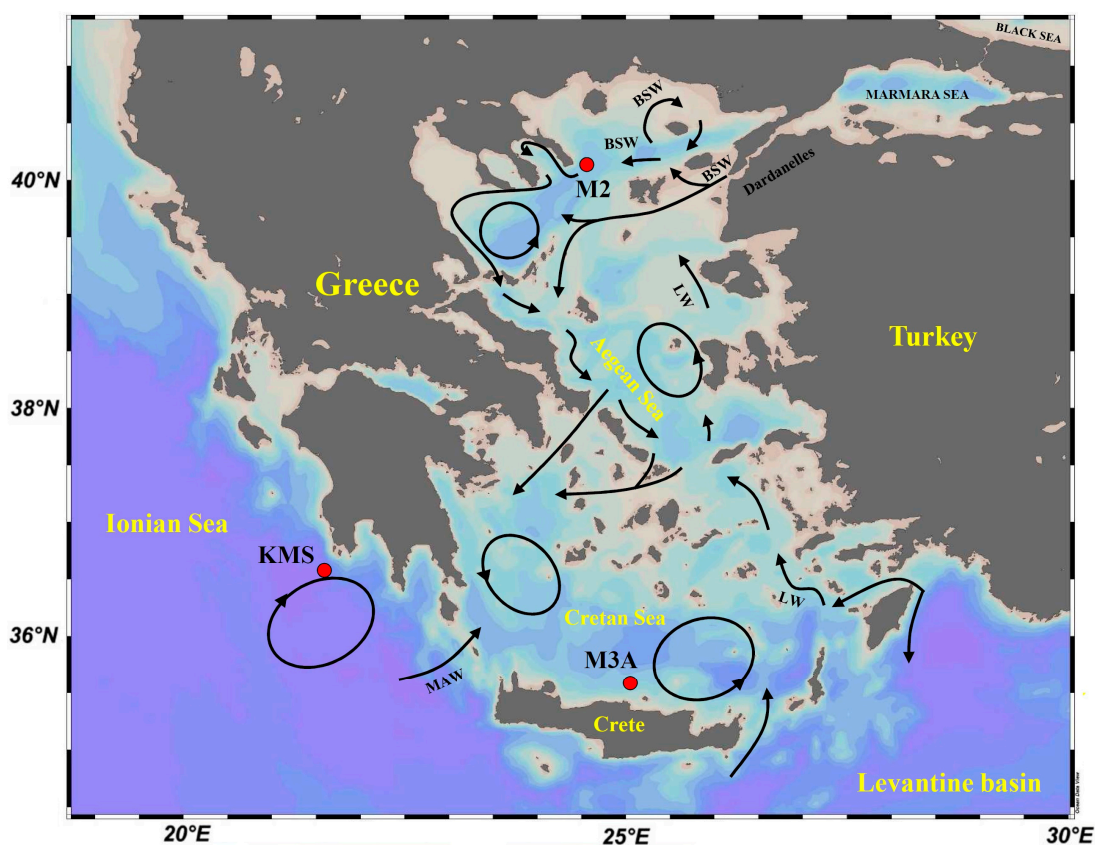
Figure 1. Location of the study sites: North Aegean Sea (M2), South Aegean/Cretan Sea (M3A), Ionian Sea (KMS) along with the main patterns of sea water surface circulation (BSW: Black Sea water, LW: Levantine water, MAW: modified Atlantic water).

The Cretan Sea is the deepest (~2500 m) and largest basin of the south Aegean Sea. It exhibits ultra-oligotrophic characteristics and low primary productivity rates, with maximum values during winter–early spring [35]. In contrast to the north Aegean Sea, the region lacks fluvial inputs, while direct interaction with the north Aegean Sea is limited to the top 400 m of the water column. The upper water column consists of the warm, saline Levantine surface water (up to ~100 m depth), the low-salinity modified Atlantic water at subsurface depths, and quantities of BSW mostly in its western part. Below ~50–100 m,

low-salinity Atlantic water enters through the Cretan Arc straits and remains at subsurface depths, especially during the summer period. Intermediate waters of local or Levantine origin occupy the intermediate (~150–600 m) layers [36].

NESTOR (KMS) site is situated in the SE Ionian Sea, including the deepest basin in the Mediterranean Sea, reaching 5264 m in depth [23]. New production mostly arises from limited events in place and time, predominantly influenced by climatological variables that create mesoscale instabilities, peaking in late winter/early spring and reaching lowest levels in summer [37,38]. The site is located in the area occupied by the permanent anticyclonic Pelops gyre, while the water column consists of a mix of water masses with varying characteristics and origins (Atlantic waters, Levantine surface and intermediate waters, Eastern Mediterranean deep waters, etc.) [23,39,40]. Of particular interest, deep-water layers in the site originate primarily in the Adriatic Sea (Adriatic deep water) and are exported to the abyssal layers of the Ionian basin through bottom arrested currents, filling the basin below ~1800 m of depth. The Aegean Sea also plays a role in deep water formation and may become a more significant deep water source than the Adriatic Sea, as demonstrated during the Eastern Mediterranean Transient (EMT) in the 1990s [39,41].

3. Materials and Methods

3.1. Sampling

All samples were collected from the three different sites located in the NEMS from January to December 2015 at various time intervals. The sampling regions were located in the mesotrophic North Aegean Sea (Athos Basin, M2 site), the ultra-oligotrophic Cretan Sea/south Aegean (M3A site), and the oligotrophic Ionian Sea (NESTOR site; KMS) (Figure 1; Table 1). Sinking particles were collected by using PPS3/3 Technicap sediment traps (0.125 m^2 collecting area, 12 receiving cups, sampling intervals of ~15 days). After the sediment traps were recovered, all samples were processed following the protocol outlined by Heussner et al. (1990) [42], which included the removal of swimmers and subsampling of collected particulate material. Subsamples for PAHs analysis were filtered on pre-weighed and pre-combusted (450 °C, 6 h) Whatman glass microfiber filters (GF/F).

Table 1. Location and deployment depth of the investigated sediment trap time series.

Sediment Trap—Code Name, Mooring Location	M2—Athos Basin North Aegean Sea	M3A Cretan Sea	KMS—Nestor Site Ionian Sea
Coordinates	39°58.16′ N, 24°43.48′ E	35°44.76′ N, 25°09.29′ E	36°2.96′ N, 21°28.93′ E
Sampling interval	01/2015–12/2015	01/2015–12/2015	01/2015–12/2015
Mooring depth (m)	500, 1000	350, 1550	700, 4300
Water column depth (m)	1050	1570	4500

3.2. Analysis and Quantitation of PAHs

For the analysis of PAHs, freeze-dried filters were initially spiked with a mixture of perdeuterated internal standards [^{2}H$_{10}$]phenanthrene, [^{2}H$_{10}$]pyrene, [^{2}H$_{12}$]chrysene, [^{2}H$_{12}$]perylene, and [^{2}H$_{12}$]benzo[*ghi*]perylene and then solvent-extracted three times by sonication with a dichloromethane:methanol mixture (4:1, *v/v*). PAHs were fractionated on a silica column, applying a modified protocol after Gogou et al. (1998) [43]. PAHs were eluted with 10 mL *n*-hexane/toluene (9:1, *v/v*). The fraction was concentrated by vacuum rotary evaporation and transferred to a 1.5 mL amber vial, and the excess solvent was evaporated under a gentle nitrogen stream.

Instrumental analysis was carried out by gas chromatography-mass spectrometry (GC-MS) on an Agilent 7890 GC (Agilent Technologies, Inc., Santa Clara, CA, USA), equipped with an HP-5MS capillary column (30 m × 0.25 mm i.d. × 0.25 μm phase film) (Supelco,

Inc., Bellefonte, PA, USA), coupled to an Agilent 5975C MSD using a selected ion monitoring (SIM) acquisition program. The oven temperature was first maintained at 60 °C for 2 min, increased to 80 °C at a rate of 25 °C/min, then raised to 300 °C at a rate of 5 °C/min and eventually sustained at 300 °C for 6 min [26]. Quantification of individual compounds was based on the internal standards added at the beginning of the analytical procedure. The response factors of the different compounds were determined by injecting a standard solution of these compounds (purchased from Dr. Ehrenstorfer GmbH, Augsburg, Germany) spiked with the internal standards.

The mean recoveries of the deuterated internal standards were: 78% for $[^2H_{10}]$phenanthrene, 91% for $[^2H_{10}]$pyrene, 89% for $[^2H_{12}]$chrysene, 94% for $[^2H_{12}]$perylene, and 86% for $[^2H_{12}]$benzo[*ghi*]perylene. The detection limits of the individual compounds were calculated to range from 0.18 ng g^{-1} for the low molecular weight PAHs to 0.6 ng g^{-1} for the heavier ones. The accuracy of the PAH determination was evaluated by analyzing a National Institute of Standards (NIST) standard reference sediment SRM 1941a (Organics in Marine Sediment). The determined values ranged between 93% and 106% of the certified values. The precision in the analysis of the samples, evaluated in terms of repeatability of the experimental results ($n = 7$) and expressed in terms of relative standard deviation, ranged from 1.7% to 5.3%. Procedural blanks run every four samples and field blanks were found to be free of contamination in all cases.

Fourteen parent (unsubstituted) PAHs included in lists of priority chemical pollutants (EPA-US) along with the methylated homologs of dibenzothiophene, phenanthrene, pyrene, and chrysene were determined. PAH compounds and their corresponding abbreviations used in the text are as follows: fluorene (Fl); dibenzothiophene (DBT); methyldibenzothiophenes (C_1-DBT); dimethyldibenzothiophenes (C_2-DBT); phenanthrene (Phe); methylphenanthrenes (C_1-Phe); dimethylphenanthrenes (C_2-Phe); trimethylphenanthrenes (C_3-Phe); anthracene (Anth); retene (Ret); fluoranthene (Flth); pyrene (Pyr); methylpyrenes (C_1-Pyr); dimethylpyrenes (C_2-Pyr); benz[*a*]anthracene (BaA); chrysene/triphenylene (Chry/Tri); methylchrysenes (C_1-Chry); dimethylchrysenes (C_2-Chry); benzo[*b/j/k*]fluoranthene (BFlths); benzo[*e*]pyrene (BeP); benzo[*a*]pyrene (BaP); perylene (Per); indeno [1,2,3-*cd*] pyrene (IndP); benzo[*ghi*]perylene (BgP); and dibenz[*a,h*]anthracene (DBA). TPAH$_{25}$ refers hereafter to the total sum of monitored compounds.

Average PAH concentrations are expressed as time-mass flux weighted means, accounting for the temporal variability of mass flux and the non-constant sampling interval. The formula used is PAH$ftw = \sum PAHiFiTi / \sum FiTi$, where PAH$ftw$ represents the time-flux weighted concentration for a given compound, *PAHi* and *Fi* are the measured PAH concentration and mass flux for sample *i*, and *Ti* is the sampling duration of sample *i* [26,44].

3.3. Analysis of Particulate Organic Carbon (POC), Stable Isotope of Carbon ($\delta^{13}C$), and Elemental Carbon (EC)

For the determination of particulate organic carbon (POC), total nitrogen (TN), and stable isotopic composition of POC (δ^{13}C-POC), subsamples of ~8 mg of sinking particulate matter were filtered through pre-combusted (450 °C, 6 h) and pre-weighed glass-fiber filters (GF/F), which were then stored at −20 °C in the dark until further analysis. Molar TN/POC ratios were also calculated. For the elimination of inorganic carbon, filters were firstly treated with HCl 2N to prevent "explosive" sample loss during reaction, with more concentrated acid added in the next step, consisting of repeated additions of HCl 6N with 60 °C drying steps in between, until no further effervescence was noticed [45].

The POC contents and δ^{13}C stable isotopic composition were determined at the Stable Isotope Facility at the University of California Davis (Davis, California, USA) using a PDZ Europa ANCA-GSL elemental analyzer coupled to a PDZ Europa 20-20 isotope

ratio mass spectrometer (Sercon Ltd., Chesire, UK). Analysis of sediment trap material for elemental carbon (EC) was performed by using the Thermal-Optical Transmission (TOT) technique [46] on a Sunset Laboratory Dual-Optical Carbonaceous Analyzer (Sunset Laboratory, Inc., Portland, OR, USA), as described in detail by Theodosi et al. (2010) [47].

3.4. Statistical Analysis

The sources of PAHs in settling particulate matter in the studied areas were investigated using the positive matrix factorization (PMF) method, which was implemented due to the potential limitations of the isomeric PAH diagnostic indices/ratios (see discussion below in Section 5.2). The PMF method is a valuable statistical technique used to identify source profiles and determine their contributions. It achieves this by decreasing the complexity of datasets and combining species and source contributions through weighted least squares regression. The PMF model postulates that the concentration of each PAH compound in every sample may be expressed as the aggregate of the compound's emission concentration from the source and the contributions from the source for each sample [48]. The results are limited to only include positive source contributions, ensuring that their interpretation is relevant in a physical sense [49]. The PMF model was implemented using the EPA PMF 5.0 software provided by the U.S. Environmental Protection Agency (EPA). The model utilized PAH concentrations and their accompanying uncertainties, which were calculated during the analytical determination, as input. The PMF model was also applied in order to investigate the processes affecting the spatial variability of PAH export in the studied areas but, in this case, considering individual PAH fluxes as input data (see discussion in Section 5.3).

Principal component analysis (PCA) [50] was additionally performed in order to identify the dominant factors of covariance within the dataset and thus the main drivers of PAH export in the studied sites. The observations included 68 sediment trap samples collected during the study period. The 18 variables considered refer to bulk properties (total mass flux (TMF) and fluxes of POC, EC, $CaCO_3$, lithogenic, opal, C/N ratio, and $\delta^{13}C$), environmental conditions (sea surface temperature (SST), Chlorophyll-a), determined PAH flux data ($TPAH_{25}$, $\sum$Phe, and $\sum$COMB) and a set of selected lipid biomarkers fluxes employed to assess the relative significance of natural vs. anthropogenic, marine and land-derived sources of settling particulate matter, along with the food web dynamics in the overlying water column, as described by Pedrosa et al. (2015) [51] and Parinos et al. (2024) [52].

The set of selected lipid biomarkers includes the fluxes of (i) terrestrial *n*-alkanes ($\sum$TerNA), (ii) the unresolved complex mixture of aliphatic hydrocarbons (UCM) indicative of anthropogenic inputs, including degraded petroleum hydrocarbons and combustion by-products, (iii) the carbon preference index of long-chain *n*-alkanes (CPI_{NA}, $Cn \geq 25$) indicating a higher odd-to-even ratio ($CPI_{NA} \geq 4$) in terrestrial plants [53,54] and ~1 in fossil fuels [55], (iv) cholesterol (cholest-5-en-3β-ol) associated with the existence of marine consumers such as zooplankton, and (v) the sum of the fluxes of selected sterols of marine algal origin ($\sum$Phyto) indicative of their source organisms, including brassicasterol (24-methylcholest-5,22-dien-3β-ol; diatoms), dinosterol (4α,23,24R-trimethyl-5α-cholest-22-en-3β-ol; dinoflagellates) and C_{30} diols/keto-ols (microalgae).

The selected lipid biomarker fluxes were determined in all collected samples following previous protocols [26,43] and were only considered in the PCA analysis; thus, their distribution trends are not further discussed. Bulk parameters fluxes (TMF, $CaCO_3$, lithogenic, and opal) are reported by Nikolopoulou et al. (2024) [31]; all satellite environmental data (Chl-a, precipitation, SST; Figure 2) were obtained from the National Aeronautic and Space Administration (NASA) Giovanni website (https://disc.gsfc.nasa.gov/ (accessed

on 23 November 2024)) and the Copernicus Marine and Environment Monitoring Service (CMEMS) (http://www.marine.copernicus.eu (accessed on 8 November 2024)).
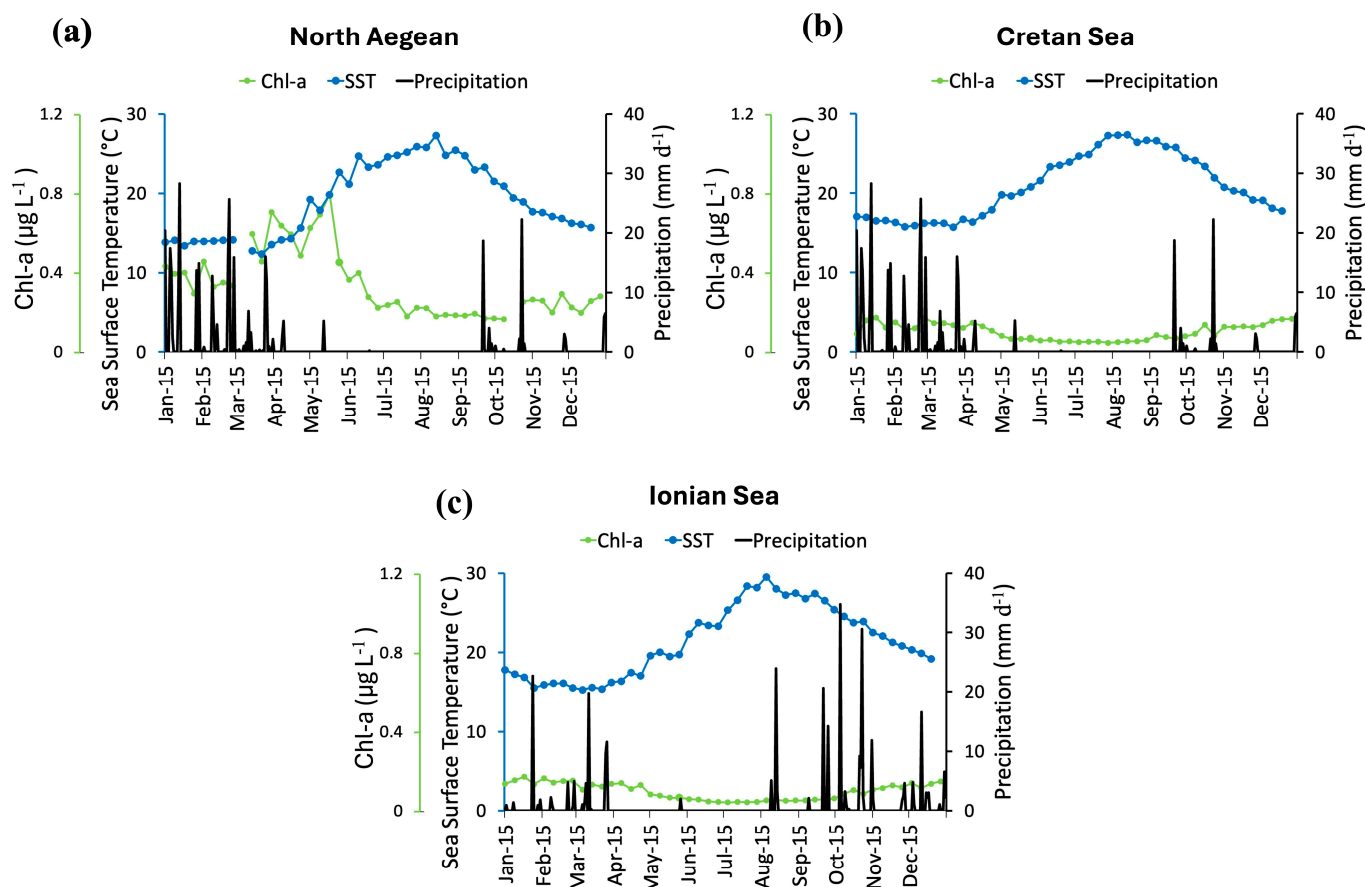

Figure 2. Environmental parameters of Chlorophyll-*a* (Chl-*a*), sea surface temperature (SST), and precipitation, concerning the study areas for the total study period; (**a**) North Aegean; (**b**) Cretan; and (**c**) Ionian Seas.

The SST data product used in this study is the SST_MED_SST_L4_REP_OBSERVATIONS _010_021 available online at https://data.marine.copernicus.eu/product/SST_MED_SST_L4 _REP_OBSERVATIONS_010_021/description (accessed on 8 November 2024), while the Chl-a data product is OCEANCOLOUR_MED_BGC_L4_MY_009_144, with variable L4 interpolated (cloud-free) data available at https://data.marine.copernicus.eu/product/OCEANCOLOUR_ MED_BGC_L4_MY_009_144/description (accessed on 8 November 2024).

Prior to the PCA, the data were normalized to the flux total, and the centered log ratio (or log contrast) transformation was applied to this compositional dataset. This transformation involved dividing by the geometric mean of the flux-normalized sample, followed by a log transformation. These steps ensured the resulting PCA dataset was free from negative bias and closure effects. Data were then auto-scaled to create a dataset in which each variable had equal weight, and the average concentration and total concentration were the same for each sample [56]. A subroutine called Varimax rotation was applied to the first three factors to maximize or minimize loadings within each factor, thereby simplifying the visual interpretation of PCA projections. PCA was performed using SPSS Statistics software v.17.0.

4. Results

4.1. Molecular Composition of PAHs

For the molecular profiles of the studied PAHs, phenanthrene and its alkylated derivatives predominate amongst low-MW (molecular weight) PAHs (≤ 3 aromatic rings), with their sum ($\sum$Phe) accounting for $41 \pm 6\%$ of the total PAHs. The sum of high-MW parent PAHs ($\geq$four aromatic rings) of predominantly pyrolytic origin [57], referred to hereafter as $\sum$COMB, represent $34 \pm 6\%$ of the total PAHs, with benzofluoranthenes, benzo[ghi]perylene, and, to a lesser degree, indeno[1,2,3-*cd*]pyrene and benzo[a]anthracene being dominant (Figure 3). However, distinct characteristics are noted for the studied PAHs' molecular profiles between the studied areas.
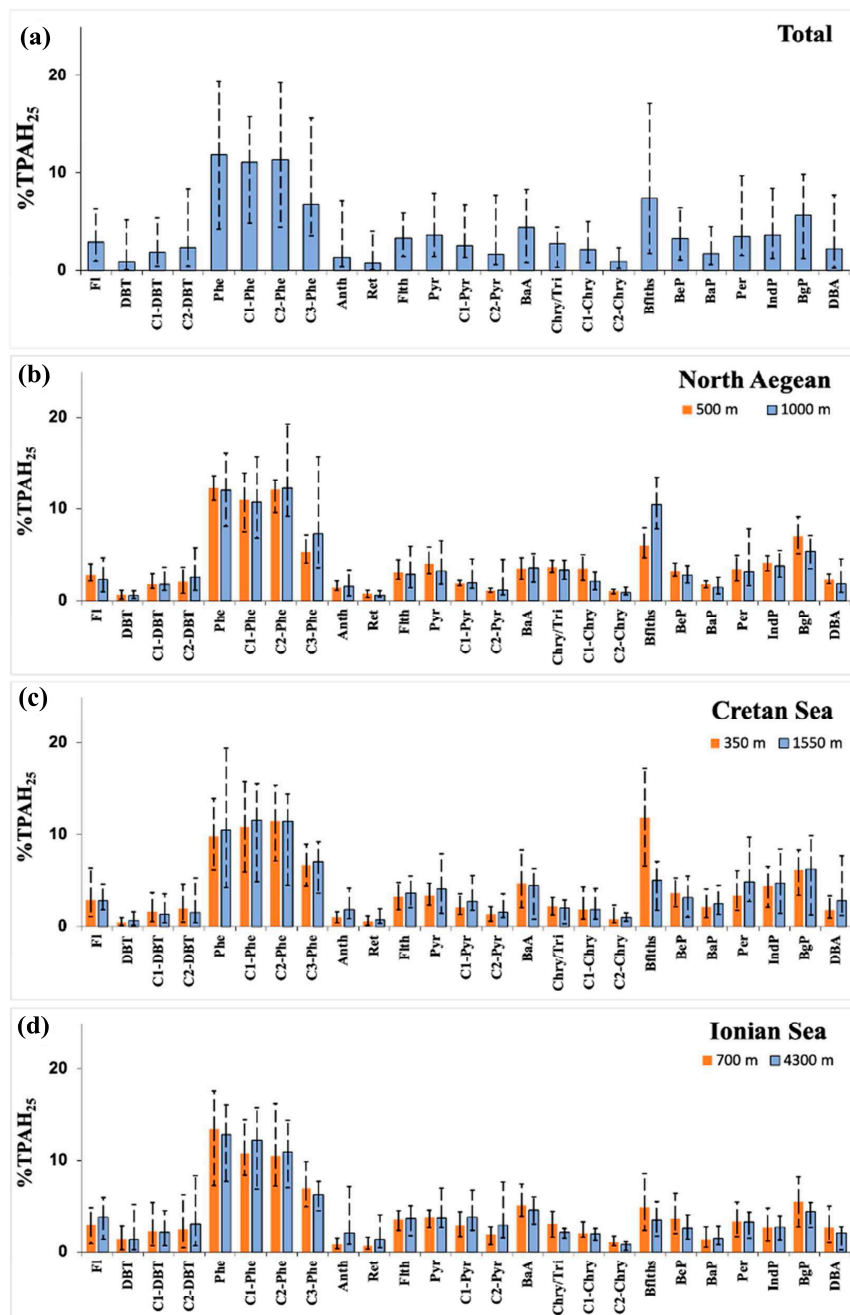

Figure 3. Molecular profiles of PAHs in sinking particles at the corresponding depths with mean abundances normalized as percentage of the total sum of PAHs monitored (%TPAH$_{25}$) along with min-max deviation lines for the: (**a**) Total study area; (**b**) North Aegean; (**c**) Cretan; (**d**) Ionian Seas. For PAH abbreviations, see Section 3.2.

The molecular profiles of PAHs in sinking particles at 500 m and 1000 m depth in the north Aegean Sea are illustrated in Figure 3b. Phenanthrene and its alkylated homologs dominated amongst three-ring compounds, maximizing, however, at C_2-Phe over the parent compound, which ranged between 63 and 83%, $71 \pm 5\%$ on average, of $\sum$MPhe, and 33 to 54%, $42 \pm 6\%$ on average, of $TPAH_{25}$. High-MW parent compounds ($\geq$four rings) were dominated by benzofluoranthenes, benzo[*ghi*]perylene, indeno[1,2,3-*cd*]pyrene, and perylene. Their sum, $\sum$COMB, ranged between 25 and 40%, averaging $33 \pm 4\%$ of $TPAH_{25}$ (Table 2).

Table 2. Ranges and median values (in parentheses) of determined PAH concentrations and fluxes.

	$TPAH_{25}$ (ng g^{-1})	$\sum$COMB (ng g^{-1})	$\sum$Phe (ng g^{-1})	$TPAH_{25}$ (ng m^{-2} d^{-1})	$\sum$COMB (ng m^{-2} d^{-1})	$\sum$Phe (ng m^{-2} d^{-1})
North Aegean (M2)						
500 m	256–476 (372)	101–152 (131)	89–209 (152)	82.6–407 (120)	32.8–130 (41.2)	28.8–179 (49.9)
1000 m	297–807 (379)	94.1–177 (121)	101–223 (162)	38.5–477 (169)	13.7–127 (58)	15.4–258 (60.2)
Cretan Sea (M3A)						
350 m	189–852 (362)	79.5–281 (132)	67.6–334 (138)	17.5–93.9 (35.1)	5.23–39.5 (13.1)	6.66–33.6 (13.4)
1550 m	247–742 (414)	64.7–389 (146)	106–334 (136)	9.49–63.6 (25.2)	3.89–22.2 (10.2)	4.07–30.4 (10.3)
Ionian Sea (KMS)						
700 m	202–654 (340)	74.5–234 (121)	80.5–267 (142)	7.26–59.6 (28.2)	2.92–17.5 (10.2)	2.4–29.1 (10.8)
4300 m	279–834 (442)	92.6–172 (146)	80.2–310 (196)	5.48–71.4 (14.6)	1.68–21.7 (4.64)	2.25–33.8 (7.28)
Total dataset	189–852 (375)	64.7–389 (128)	67.6–334 (154)	5.48–477 (37.9)	1.68–130 (14.2)	2.25–258 (15.0)

The molecular profiles of PAHs in the Cretan Sea sinking particles at 350 m and 1550 m depths (Figure 3c) were again dominated by the parent phenanthrene rather than its alkylated derivatives. Methylated phenanthrenes ranged between 62 and 83%, $75 \pm 6\%$ on average, of $\sum$MPhe and 17 to 54%, $39 \pm 8\%$ on average, of $TPAH_{25}$, followed by high-MW parent compounds ($\geq$four rings) which were dominated by benzo[*ghi*]perylene and indeno[1,2,3-*cd*]pyrene, benzo[*a*]anthracene, perylene, and DBA. The sum of $\sum$COMB ranged between 24 and 52%, averaging $36 \pm 6\%$ of the total PAHs (Table 2).

In the Ionian Sea sediment trap, the molecular profiles of PAHs in sinking particles at 700 m and 4300 m depths were dominated by phenanthrene and its alkylated homologs (three-rings), maximizing, however, at the parent phenanthrene rather than the alkylated compounds, which ranged between 57 and 82%, $68 \pm 6\%$ on average, of $\sum$MPhe and 26 to 50%, on average, of $TPAH_{25}$. $\sum$COMB ranged from 21 to 45%, averaging $33 \pm 6\%$ of $TPAH_{25}$, being dominated by benzo[*ghi*]perylene, pyrene, benzo[*a*]anthracene, and benzofluoranthenes, although relatively high contributions for chrysene and its homologs were also noted in the case of the 700 m water column depth sediment trap (Figure 3d).

4.2. PAH Concentrations and Fluxes

The concentrations and fluxes of PAHs determined in the studied sites are depicted in Table 2. The concentrations of $TPAH_{25}$ in sinking particles ranged from 189–852 ng g^{-1} (median 375 ± 165 ng g^{-1}). $\sum$COMB concentrations ranged from 64.7–389 ng g^{-1} (median 128 ± 53.2 ng g^{-1}), while $\sum$Phe ranged from 67.6–334 ng g^{-1} (median 154 ± 64.6 ng g^{-1}). The $TPAH_{25}$ flux in sinking particles ranged from 5.48 to 477 ng m^{-2} d^{-1} (median 37.9 ± 96.7 ng m^{-2} d^{-1}) during the study period. $\sum$COMB ranged from 1.68–130 ng m^{-2} d^{-1} (median 14.2 ± 29.2 ng m^{-2} d^{-1}), while $\sum$Phe ranged from 2.25–258 ng m^{-2} d^{-1} (median 15 ± 46 ng m^{-2} d^{-1}).

In the North Aegean Sea at 500 m depth, the $TPAH_{25}$ concentrations ranged from 256–476 ng g^{-1} (median 372 ± 68.8 ng g^{-1}) while at 1000 m depth, they varied from 297–807 ng g^{-1} (median 379 ± 120 ng g^{-1}). The $\sum$COMB concentrations ranged from 101–152 ng g^{-1} (median 132 ± 16.4 ng g^{-1}) at 500 m and from 94.1–177 ng g^{-1} (median 121 ± 19.9 ng g^{-1}) at 1000 m depth. Similarly, $\sum$Phe ranged from 89–209 ng g^{-1} (median

152 ± 38.3 ng g^{-1}) at 500 m and from 101–223 ng g^{-1} (median 162 ± 42.2 ng g^{-1}) at 1000 m depth. As for TPAH$_{25}$ fluxes, at 500 m depth, they ranged from 82.6–407 ng m^{-1} d^{-1} (median 120 ± 112 ng m^{-2} d^{-1}), while at 1000 m depth, they varied from 38.5–477 ng m^{-1} d^{-1} (median 169 ± 124 ng m^{-2} d^{-1}). $\sum$COMB fluxes varied from 32.8–130 ng m^{-2} d^{-1} (median 41 ± 34.4 ng m^{-2} d^{-1}) at 500 m and from 13.7–127 ng m^{-2} d^{-1} (median 58 ± 35.8 ng m^{-2} d^{-1}) at 1000 m depth. Meanwhile, $\sum$Phe fluxes varied from 28.8–179 ng m^{-2} d^{-1} (median of 49.9 ± 50.9 ng m^{-2} d^{-1}) at 500 m and from 15.4–258 ng m^{-2} d^{-1} (median of 60.2 ± 66 ng m^{-2} d^{-1}) at 1000 m depth. (Table 2).

TPAH$_{25}$ concentrations at 350 m depth in the Cretan Sea, ranged from 189–852 ng g^{-1} (median 362 ± 192 ng g^{-1}), while at 1550 m depth, they varied from 247–742 ng g^{-1} (median 414 ± 195 ng g^{-1}). $\sum$COMB concentrations ranged from 79.5–281 ng g^{-1} (median 132 ± 54.1 ng g^{-1}) at 350 m and from 64.7–389 ng g^{-1} (median 146 ± 105 ng g^{-1}) at 1550 m depth. Similarly, $\sum$Phe ranged from 67.6–334 ng g^{-1} (median 138 ± 81 ng g^{-1}) at 350 m and from 106–334 ng g^{-1} (average 136 ± 75.7 ng g^{-1}) at 1550 m depth. As for TPAH$_{25}$ fluxes, at 350 m depth, they ranged from 17.5–93.9 ng m^{-1} d^{-1} (median 35 ± 24.9 ng m^{-2} d^{-1}), while at 1550 m depth, they varied from 9.49–63.6 ng m^{-1} d^{-1} (median 25.2 ± 16.2 ng m^{-2} d^{-1}). $\sum$COMB fluxes ranged from 5.23–39.5 ng m^{-2} d^{-1} (median 13.1 ± 9.76 ng m^{-2} d^{-1}) at 350 m and from 3.89–22.2 ng m^{-2} d^{-1} (median 10.2 ± 6.52 ng m^{-2} d^{-1}) at 1550 m. Meanwhile, $\sum$Phe flux varied from 6.66–33.6 ng m^{-2} d^{-1} (median of 13.4 ± 8.32 ng m^{-2} d^{-1}) at 350 m and from 4.07–30.4 ng m^{-2} d^{-1} (median of 10.3 ± 7.8 ng m^{-2} d^{-1}) at 1550 m depth (Table 2).

Finally, in the Ionian Sea, at 700 m depth, TPAH$_{25}$ concentrations varied from 202–654 ng g^{-1} (median 340 ± 125 ng g^{-1}), while at 4300 m depth, they varied from 279–834 ng g^{-1} (median 442 ± 200 ng g^{-1}). $\sum$COMB concentrations ranged from 74.5–234 ng g^{-1} (median 121 ± 43.3 ng g^{-1}) at 700 m and from 92.6–172 ng g^{-1} (median 146 ± 28.9 ng g^{-1}) at 4300 m. Similarly, $\sum$Phe ranged from 80.5–267 ng g^{-1} (median 142 ± 44.4 ng g^{-1}) at 700 m and 80.2–310 ng g^{-1} (median 196 ± 73.8 ng g^{-1}) at 4300 m depth. As for TPAH$_{25}$ fluxes, at 700 m ranged from 2.80–58.7 ng m^{-1} d^{-1} (median $28.2 \pm 15.$ ng m^{-2} d^{-1}), while at 4300 m fluxes ranged from 5.42–70.4 ng m^{-1} d^{-1} (median 10.6 ± 23.3 ng m^{-2} d^{-1}). $\sum$COMB fluxes ranged from 2.92–17.5 ng m^{-2} d^{-1} (median 10.2 ± 4.87 ng m^{-2} d^{-1} at 700 m and from 1.68–21.7 ng m^{-2} d^{-1} (median 4.64 ± 7.83 ng m^{-2} d^{-1}) at 4300 m depth. Meanwhile, $\sum$Phe flux varied from 2.40–29.1 ng m^{-2} d^{-1} (median 10.9 ± 6.46 ng m^{-2} d^{-1} at 700 m and from 2.25–33.8 ng m^{-2} d^{-1} (median of 7.28 ± 10.1 ng m^{-2} d^{-1}) at 4300 m depth. (Table 2).

5. Discussion

5.1. Levels of PAH Contamination in the Studied Sites

The PAH levels and fluxes determined by settling the particulate matter of the studied sites exceed those previously detected in the open eastern Mediterranean Sea [20,43] but are similar to those in the open western Mediterranean Sea [4], the SW Black Sea [43], and the open Alboran Sea [58]. However, they are substantially lower compared to areas adjacent to continental regions in the Ligurian Sea and the Gulf of Lion–western Mediterranean [14,16,59,60]. Globally, the PAH levels and fluxes in sinking particles from the NEMS exceed those detected for the New Jersey coastal area (USA), Koster fjord (Sweden), and the Gaoping/Kaoping submarine canyon (Taiwan), yet are lower than those in near-surface traps at Puget Sound, Washington (USA), the Baltic Sea [61–65], and the Gulf of Mexico [66].

5.2. Sources of PAHs in Settling Particles of the Study Areas

The molecular composition of the studied PAHs (Figure 3) indicates varying contributions from (i) unburned fossil fuels (petroleum), which is mainly characterized by the prevalence of three-ring alkylated homologs (phenanthrene series) among low-MW PAHs, and (ii) the combustion/pyrolysis of fossil fuels/biomass, which is characterized by parent PAHs with > four aromatic rings [67–70]. In addition, we employed PAH diagnostic ratios that are commonly used to evaluate specific sources of PAHs in the marine environment [15]. Nevertheless, they need to be perceived with caution, since the retention of PAHs throughout transport from initial sources is mainly determined by the characteristics, sizes, and instability of their carrier particles [15,68] (and references therein). The Flth/(Flth + Pyr) ratio varied from 0.36 to 0.65, the BaA/(BaA + Chry) ratio ranged from 0.37 to 0.84, and the IndP/(IndP + BgP) ratio ranged from 0.24 to 0.51. These values indicate a combination of sources that originate from the combustion of petroleum, grass, wood, and coal for these high-MW pyrolytic PAHs [15]. In the lower MW range, evidence for the presence of PAHs produced from petroleum is indicated by the low Phe/(Phe + C_1-Phe) ratio values (<0.5) ranging from 0.38 to 0.65. In contrast, values > 0.5 suggest a relatively higher contribution of parent (pyrolytic) phenanthrene (Table 3; Figure 4).

Table 3. Ranges and average values (in parentheses) of PAH source-specific diagnostic ratios in the studied sites.

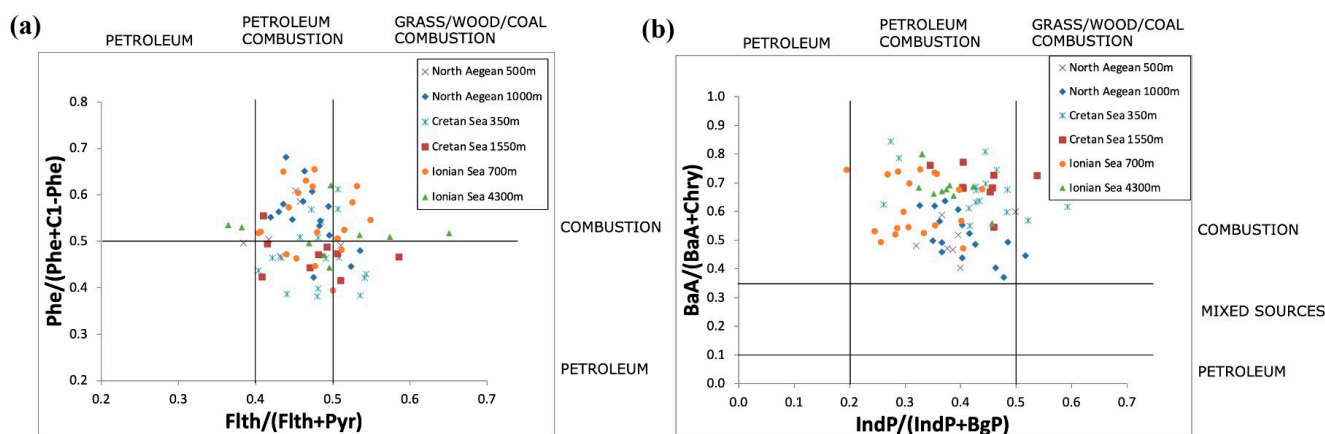|	Phe/(Phe + C_1-Phe)	Flth/(Flth + Pyr)	BaA/(BaA + Chry)	IndP/(IndP + BgP)	∑Phe/∑COMB
North Aegean (M2)					
500 m	0.47–0.61 (0.53)	0.38–0.49 (0.44)	0.40–0.59 (0.49)	0.32–0.40 (0.37)	0.99–1.38 (1.17)
1000 m	0.42–0.61 (0.53)	0.42–0.54 (0.47)	0.37–0.64 (0.51)	0.35–0.52 (0.41)	0.89–2.03 (1.33)
Cretan Sea (M3A)					
350 m	0.38–0.61 (0.47)	0.42–0.54 (0.49)	0.55–0.84 (0.66)	0.26–0.52 (0.42)	0.84–2.06 (1.08)
1550 m	0.42–0.55 (0.47)	0.41–0.59 (0.48)	0.55–0.76 (0.68)	0.35–0.54 (0.44)	0.33–1.20 (0.83)
Ionian Sea (KMS)					
700 m	0.39–0.65 (0.55)	0.36–0.65 (0.48)	0.47–0.75 (0.61)	0.24–0.44 (0.33)	0.72–1.41 (1.15)
4300 m	0.44–0.62 (0.52)	0.41–0.55 (0.47)	0.56–0.84 (0.70)	0.32–0.46 (0.37)	0.83–1.80 (1.38)

Figure 4. (**a**) The Phe/(Phe + C_1-Phe) vs. Flth/(Flth + Pyr); (**b**) the BaA/(BaA + Chry) vs. IndP/(IndP + BgP) diagnostic ratios cross plots for the studied areas (north Aegean, Cretan, and Ionian Seas), along with values corresponding to specific PAH sources following Yunker et al. (2002) [15].

To further investigate the origin of PAHs in settling particulate matter of the study areas, a positive matrix factorization (PMF) model was applied [71,72]. Figure 5 illustrates the outcomes of the PMF model. Methylated derivatives of DBT, indicative of low-MW petrogenic inputs, are predominant in Factor 1 [73], while higher MW compounds are observed to a lesser extent. Factor 2 is primarily composed of four-ring PAHs, including Pyr, Chry, and BaA, along with their methylated derivatives, with three-ring PAH contribution of a lesser degree, likely indicating petrogenic origins from petroleum sources

and/or combustion of petroleum products [71]. Factor 3 is characterized by the predominance of three-ring PAHs, such as phenanthrene, anthracene, and retene, i.e., compounds typically formed during low-temperature combustion processes, likely biomass burning (grass/wood) [74], while five-to-six-ring PAHs contribute to a lesser extent. Lastly, five-to-six-ring parent PAHs, such as Bflths, BeP, IndP, BghiP, and DBA, dominate Factor 4, suggesting an association with high-temperature combustion processes like, e.g., fuel oil combustion in engines, industrial processes, or coal burning [72].
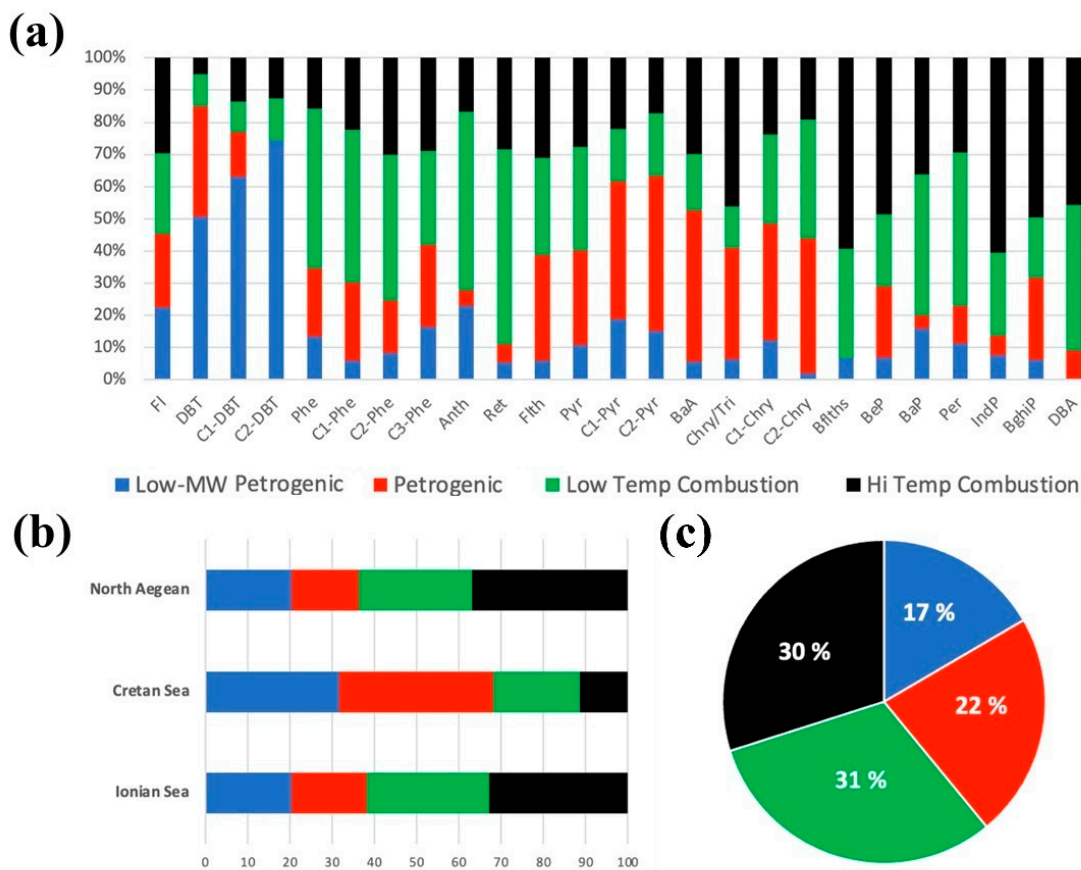
Figure 5. (**a**) Factor profiles (%TPAH$_{25}$ concentrations); (**b**) Factor contributions (avg = 1) for each study area; (**c**) relative contribution of each factor to the determined TPAH$_{25}$ concentrations.

The most prevalent PAH source, as indicated by the PMF model, was low-temperature combustion, with a relative contribution of 31%. High-temperature combustion followed, with a relative contribution of 30%, petrogenic sources and low-MW petrogenic inputs contributed 22% and 17%, respectively (Figure 5c). Thus, the reported results highlight combustion as a significant source of PAHs, accounting for up to 61%, indicating an important contribution from atmospheric inputs in the studied sites.

Indeed, the NEMS area experiences significant human-induced stress, leading to the release of significant amounts of combustion-derived PAHs, along with petroleum pollution of the marine environment due to enhanced maritime transport [75]. In addition, the NEMS is characterized by a highly concentrated network of national/international maritime shipping routes that connect the Mediterranean Sea and the Black Sea, as well as the many inhabited islands of Greece to the mainland [76]. Aeolian transport significantly contributes to the long-range transport of anthropogenic-related PAHs throughout the NEMS. The composition of PAHs in EMS aerosols highlights considerable variability due to physical and chemical factors. However, it remains rather constant in areas far from urban centers and point sources [77–80].

Upon examining the factor loadings at each location (Figure 5b), it is evident that the North Aegean and Ionian Seas have similar loadings across the factors, with low- and high-temperature combustion sources making an important contribution to the overall PAH levels (>60% in both cases). Interestingly, petrogenic/petroleum inputs are the most significant source at the Cretan Sea (~70%). This contribution could be likely attributed to several biogeochemical factors influencing the spatial variability of PAH fluxes in the studied areas, discussed in detail in Section 5.3 below.

5.3. Processes Affecting the Temporal and Spatial Variability of PAH Concentrations and Fluxes

The temporal variability of PAHs (TPAH$_{25}$, $\sum$Phe, and $\sum$COMB) concentrations and fluxes in the North Aegean, Cretan, and Ionian Seas (Figures 6 and 7) reveals distinct seasonal and depth-dependent distribution patterns, reflecting the contribution from varying sources and transport mechanisms in the studied sites. Important variation, exceeding one order of magnitude, is noted for TPAH$_{25}$ fluxes. This could result from variations in both the PAH load on particles and/or the rain of carrier particles. To further investigate, we also consider the total mass flux, along with the fluxes of organic carbon (POC), carbonates (CC), and opal, reported by Nikolopoulou et al. (2024) [31] and Skampa et al. (2020) [35].
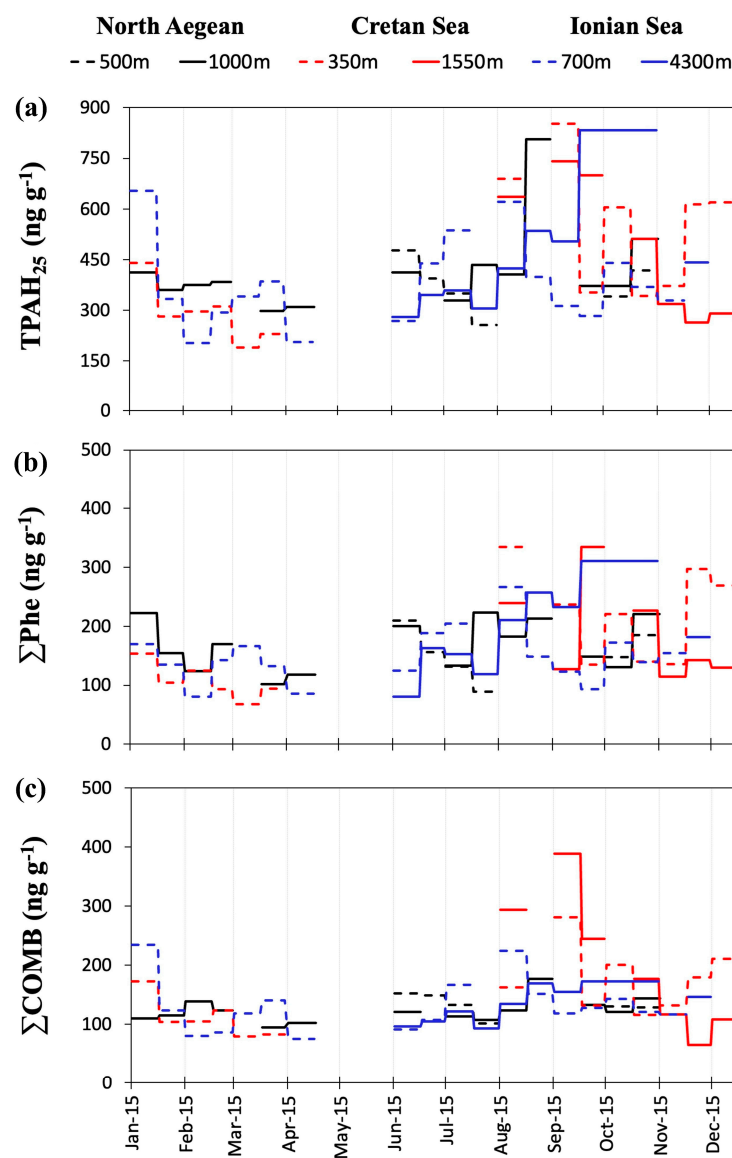

Figure 6. Time series of concentrations expressed in ng g^{-1} for (**a**) TPAH$_{25}$; (**b**) $\sum$Phe; (**c**) $\sum$COMB determined at corresponding sampling depths for the total study period.
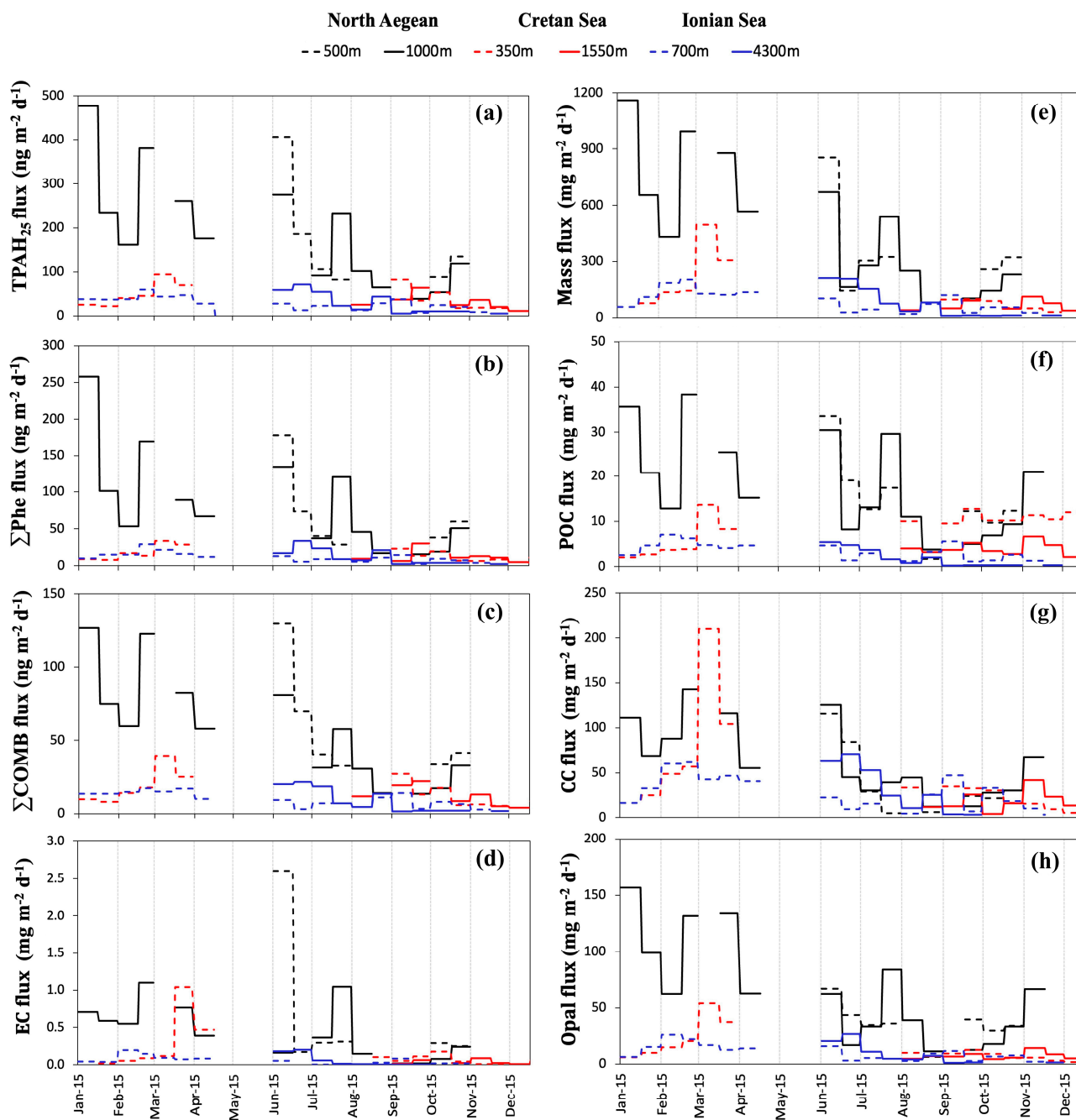
Figure 7. Time series of fluxes in the studied sites for (**a**) $TPAH_{25}$; (**b**) $\sum$Phe; and (**c**) $\sum$COMB; (**d**) elemental carbon; (**e**) total mass; (**f**) particulate organic carbon; (**g**) carbonates and (**h**) opal, determined at corresponding sampling depths for the total study period. Fluxes E, G, and H data adapted from Nikolopoulou et al. (2024) [31] and Skampa et al. (2020) [35].

In the North Aegean Sea, $TPAH_{25}$ concentrations exhibit seasonal peaks during early June and late August at 500 m and 1000 m depths (Figure 6a). The concurrent peaks observed in $\sum$Phe and $\sum$COMB concentrations during summer further highlight the contribution of both petroleum- and combustion-derived PAHs reaching the deep-sea floor (Figure 6b,c). In the North Aegean Sea, PAH fluxes exhibit their highest values (four- to five-fold higher) amongst the three sites, with the highest fluxes being recorded during winter/spring at 1000 m depth (Figure 7a), which is in agreement with TMF and biogenic components fluxes (OC, CC, and opal) (Figure 7e,f). Moreover, $\sum$Phe fluxes exceeded $\sum$COMB ones, indicating a prevalence of sources associated with unburned fossil fuels (Figure 7b,c).

Indeed, the north Aegean Sea receives enhanced petroleum inputs from continental sources through long- and medium-range transport as well as from merchant shipping and oil transportation through the Dardanelles Straits but also significant human-induced pollution from major rivers and the inflow of the Black Sea water introducing various organic contaminants [52]. However, the prevalence of petroleum-derived sources over combustion ones in the region also emphasizes the enhanced preservation of low-MW petrogenic PAHs during their downward transport through the water column. This could be likely attributed to the mesotrophic character of the North Aegean Sea due to the inflow of BSW and riverine waters, which enhances the inorganic and organic nutrient content in this area [3,81,82], and the consequent increased Chl-a recorded values (Figure 2a) and relatively high TPAH$_{25}$ fluxes (see the discussion below in Section 5.4). Low-MW petrogenic compounds, which are more prevalent in the dissolved phase, are efficiently removed by organic-rich particles such as phytoplankton and fecal pellets, resulting in a shorter residence time and thus a limited potential for their degradation in the upper water column, thus facilitating their preservation during downward transport [4,26,58,59,83].

In the Cretan Sea, TPAH$_{25}$ concentrations exhibit seasonal peaks during early August and early September at 350 m and 1550 m depths (Figure 6a). Similar temporal patterns are observed in $\sum$Phe and $\sum$COMB, with peaks reflecting petrogenic and pyrolytic contributions. At 350 m depth in August, $\sum$Phe slightly exceeds $\sum$COMB, suggesting that dominant petrogenic sources are likely associated with unburned fossil fuels (Figure 6b,c). The Cretan Sea displayed three distinct peaks in PAH fluxes, i.e., in early spring at 350 m and early fall 2015 at both depths. This coincides with peaks for both $\sum$Phe and $\sum$COMB fluxes, indicating increased pollutant inputs from both pyrolytic and petrogenic origins (Figure 7b,c). Additionally, TMF and biogenic component fluxes (OC, CC, and opal) showed a maximum in spring at 350 m, indicating the presence of a process that increases the export of all biogenic constituents and associated PAHs (Figure 7d–f).

In the Ionian Sea, TPAH$_{25}$ concentrations show distinct peaks occurring outside the productive season, in early January, July, and August, at 700 m and late August and September at 4300 m depths (Figure 6a). $\sum$Phe and $\sum$COMB exhibit similar seasonal patterns indicative of increased pollutant contributions from both pyrolytic and petrogenic origins (Figure 6b,c). In the Ionian Sea, PAH fluxes exhibited the lowest average total vertical fluxes compared to the other examined sites, with distinct peaks observed in late winter/early spring 2015 at 700 m depth and during summer 2015 at 4300 m depth (Figure 7b,c). While the Ionian Sea is not more oligotrophic than the Cretan Sea, its abyssal layer (5264 m depth) results in the significant degradation of PAHs. The increased water column depth extends the residence time of these compounds, allowing for more extensive degradation. The concurrent peak in POC flux underscores its role as an effective carrier for PAHs, consistent among other studies [4,14,58]. $\sum$Phe and $\sum$COMB peaks exhibit similar seasonal patterns aligning with winter and spring combustion-related emissions.

To further investigate the significance of mechanisms affecting the spatial variability of PAH export in the studied areas, a positive matrix factorization (PMF) model was applied, as in the case of major PAH source appreciation above but this time considering individual PAH fluxes as input data. Based on the PMF analysis (Figure 8), four distinct factors were identified.

In Factor 1, methylated derivatives of DBT are predominant, followed by Phe, Pyr, and their methylated derivatives, although to a lesser extent, reflecting primarily low-MW petrogenic inputs, while higher MW PAHs (five to six rings) are nearly absent. The Factor 1 contribution (Figure 8b) is predominant in the North Aegean Sea, and thus, it could be likely representing the preservation of petroleum-related PAHs due to their high association with OC leading to efficient transport to depth [4]. Factor 2 consists mainly of PAHs with five to

six rings, which are typically produced during high-temperature combustion processes, with a smaller contribution from three-to-four-ring PAHs such as Chry, Anth, Ret, and DBT, likely representing char carbon dynamics on the export of PAHs in the three studied sites.
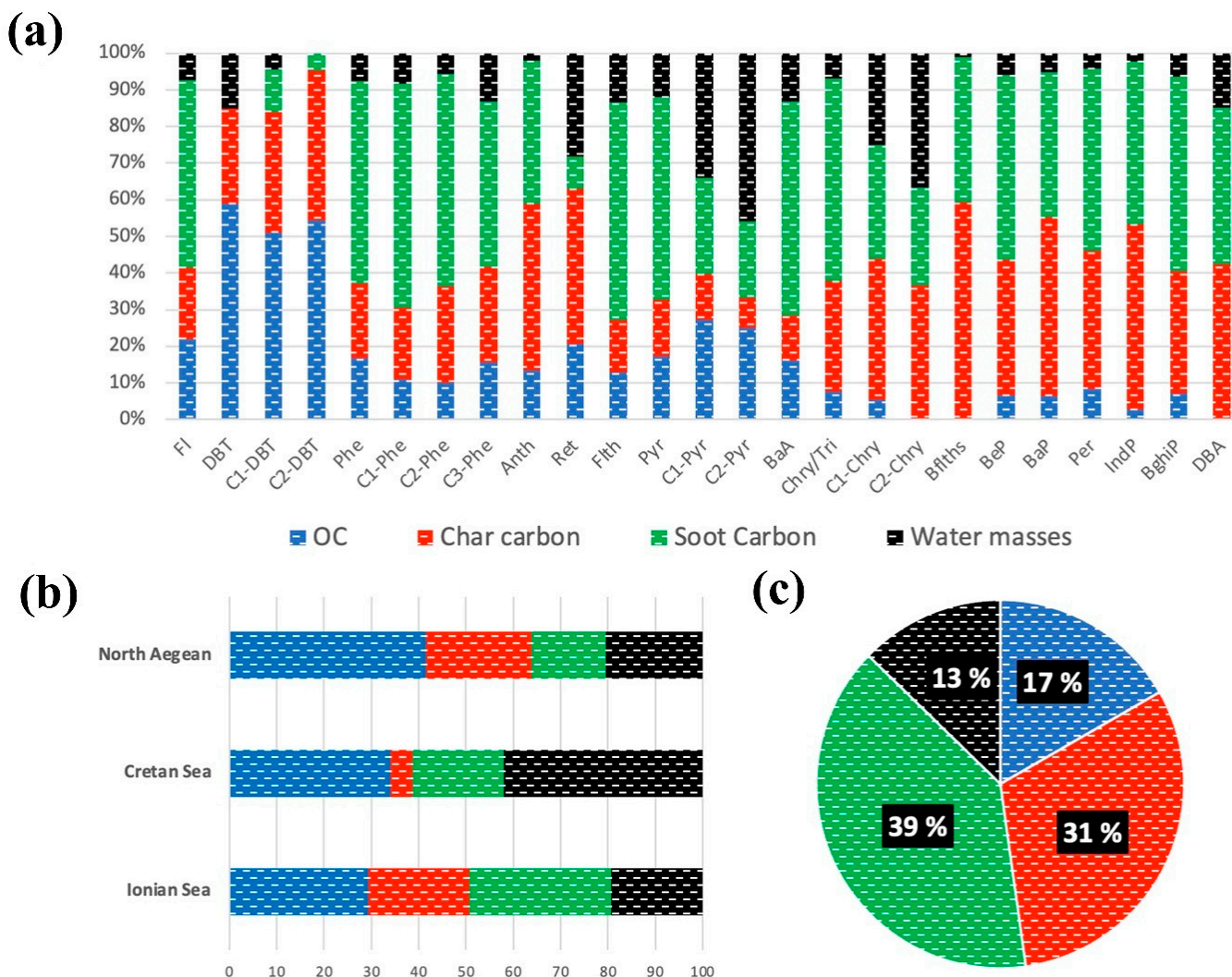

Figure 8. (**a**) Factor profiles (% of TPAH$_{25}$ flux); (**b**) factor contributions (avg = 1) for each study area; (**c**) relative contribution of each factor to the determined TPAH$_{25}$ fluxes.

Factor 3 is primarily characterized by four-ring PAHs, along with Phe and its methylated derivatives, which are generally formed during low-temperature combustion processes, with a lesser contribution from five-to-six-ring PAHs, likely attributed to soot carbon as a process determining PAH export. Char/soot carbon have been widely documented across the literature to protect PAHs from degradation during their transport from the original sources, whether through atmospheric or aquatic pathways and through the water column [15,20,26,77,84,85].

Factor 4 is dominated by methylated derivatives of Pyr and Chry, with a smaller contribution from three-ring PAHs, such as DBT, Phe, and Ret, and a minor contribution from five-to-six-ring PAHs, indicating a molecular signal linked to petroleum-related inputs. Interestingly, Factor 4 predominates in the Cretan Sea (Figure 8b), consistent with the predominance of a fossil-related petrogenic signal, as reflected in the case of major PAH source appreciation, considering PAHs concentrations through the PMF analysis above (Factors 1 and 2, Figure 5b). This pattern could likely be attributed to the main water mass circulation patterns and the Aegean's general cyclonic surface circulation. Mesoscale

activity and strong bottom currents at the Cyclades Plateau play a significant role in driving the increased contribution of phenanthrene-related petrogenic inputs through advective pathways in the southern Aegean and Cretan Sea [52]. Thus, Factor 4 could be likely attributed to the influence of water mass circulation patterns as a process affecting the spatial variability of PAH fluxes in the studied sites.

Overall, considering the above, the atmospheric deposition of char and soot carbon seem to constitute the most significant processes affecting the spatial variability of PAH fluxes in the studied sites, contributing on average 39% and 31%, respectively, followed by organic carbon flux (17%) and the influence of water masses circulation patterns (13%) (Figure 8c).

5.4. Drivers of PAH Export to Deep Waters of the NEMS

To further evaluate the influence of particle composition and fluxes on the downward transport of PAHs at the studied sites, PCA was also conducted. Three main PCs, responsible for 76.5% of the total variance, were identified (Table 4; Figure 9).

Table 4. Factor loadings in the three main identified PCs for all parameters employed in PCA analysis. Significant positive/negative loading values (>0.6) in each PC are highlighted following the layout of Figure 9, i.e., PC1—blue; PC2—green; and PC3—brown color.

Parameter	PC1 (57.7%)	PC2 (11.9%)	PC3 (6.9%)
TMF	0.949	0.200	0.170
POC Flux	0.842	0.266	0.020
$CACO_3$ Flux	0.869	0.058	−0.007
Lithogenic Flux	0.920	0.226	0.218
Opal Flux	0.931	0.226	0.194
EC Flux	0.904	0.111	0.148
C/N Ratio	−0.084	−0.042	−0.777
$\delta^{13}POC$	−0.590	−0.125	−0.499
SST	−0.460	0.117	−0.437
Chlorophyll-a	0.635	0.149	0.633
$TPAH_{25}$ Flux	0.913	0.240	0.158
$\sum$COMB Flux	0.925	0.246	0.137
$\sum$PHE Flux	0.892	0.249	0.190
$\sum$TerNA Flux	0.555	0.701	0.252
UCM Flux	0.192	0.761	0.110
Cholesterol Flux	0.140	0.704	−0.145
$\sum$Phyto Flux	0.344	0.729	−0.166
CPI_{NA}	−0.107	0.764	0.396

PC1 explains 57.7% of the total variance, with strong positive loadings on all bulk parameters, PAHs, and EC, verifying that biogenic particle fluxes are the primary driver for the downward transfer of bulk PAHs in the studied sites, in agreement with previous observations [4,14,26,58,59]. PC1's positive association with elemental carbon further suggests that anthropogenic sources, like soot/char particles transported from the atmosphere, further contribute to the export dynamics of, most likely pyrolytic, PAHs.

PC2 accounted for 11.9% of the variance, with strong positive loadings on $\sum$TerNA, UCM, $\sum$Phyto fluxes, and CPI_{NA}, likely indicating the influence of land-derived organic carbon on particle fluxes in the studied areas deriving from riverine runoff and/or atmospheric deposition. The positive loading of cholesterol within PC2 likely indicates the role of secondary production on POC and associated PAH export in the studied areas.

Lastly, PC3 accounted for 6.9% of the total variance, with positive loadings on chlorophyll-a and CPI_{NA} and negative to C/N ratio, likely reflecting the role of phytoplankton-derived POC, shaped by seasonal productivity and regional hydrographic features. The negative loadings on $\delta^{13}C$, C/N ratio, and $CaCO_3$ fluxes within PC3 indicate that the POC associated with this PC is isotopically lighter and less carbonate-rich,

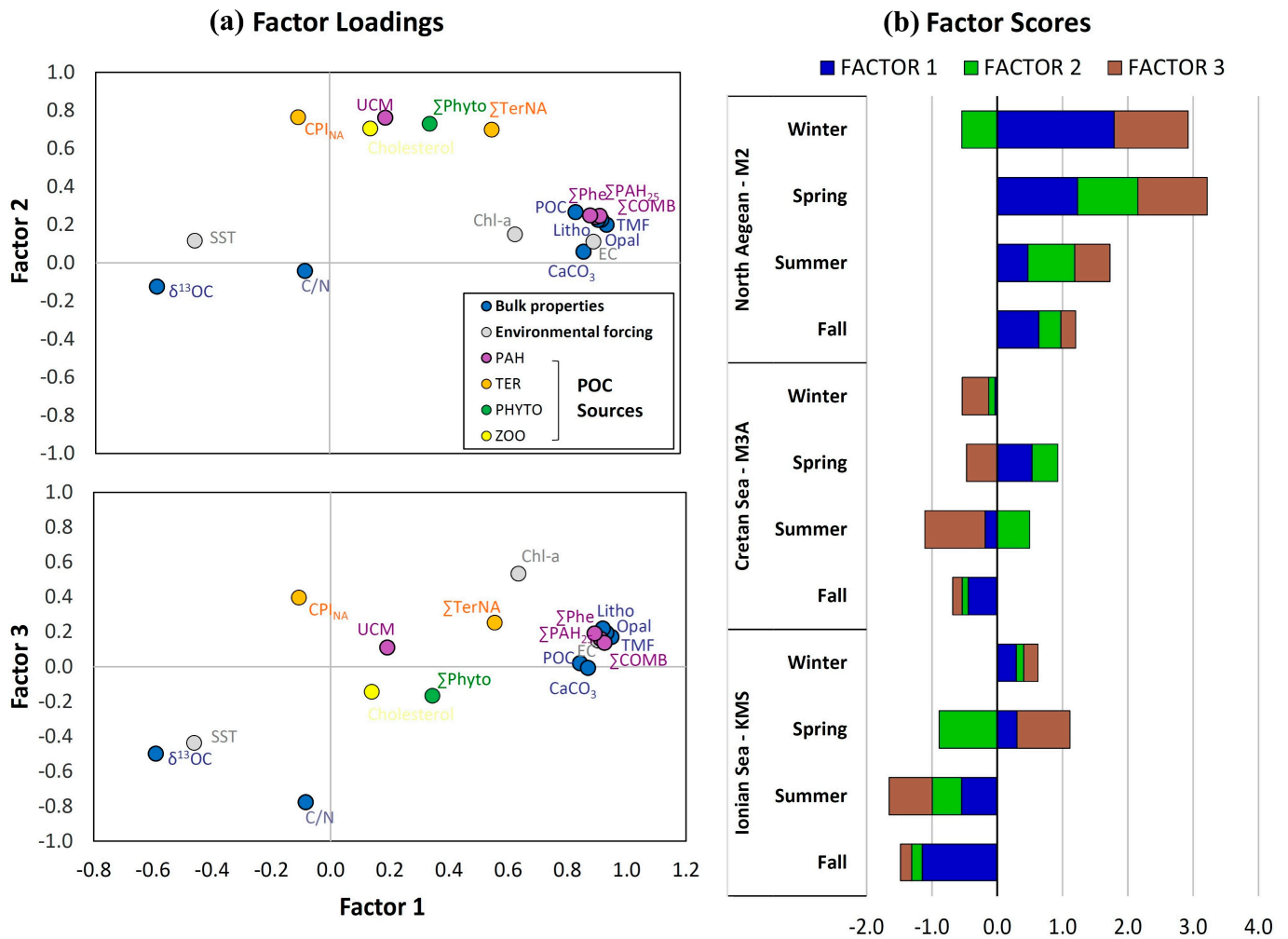which is consistent with organic matter produced by non-calcifying phytoplankton, such as diatoms [86].

Figure 9. PCA results. (**a**) Factor loadings for environmental forcing, bulk properties, PAHs and lipid biomarkers for the collected sinking particles; (**b**) Plot of main factor scores for sinking particles identified for each station and season.

The North Aegean Sea presents the highest positive scores for all PCs, with the exception of PC2 during winter (Figure 9). During the studied period, the late February–March 2015 peak in the flux of all biogenic components (Figure 7e–h), dominated by coccolithophores [35], coincides with high values of precipitation (Figure 2a) and could likely result in the fertilization with nutrients of the upper water column during this interval. During summer, the BSW inflow in the area reaches maximum rates [87,88], enriching the North Aegean Sea waters with nutrients in the photic layer and leading to a siliceous bloom (Figure 7h), which drives the secondary peak of POC and associated PAH compounds (Figure 7a,f). The peak flux of EC in early June 2015 at 500 m depth (Figure 7d) further indicates an additional force contributing to the summer siliceous bloom, likely driven by increased nutrient inputs via atmospheric deposition and also enhancing the export of pyrolytic PAHs (Figure 7c) [19].

While the highest PC1 positive scores are observed in the North Aegean Sea, notable high PC1 loadings in spring samples from the Cretan Sea indicate relatively enhanced productivity during this season compared to other seasons, typical for the Eastern Mediterranean Sea blooming periods. The maxima for CC flux (Figure 7g) indicate a coccolithophore bloom driving POC and associated PAH export. Enhanced precipitation

(Figure 2b) and elevated EC flux (Figure 7d) likely indicate increased aerosol inputs through wet atmospheric deposition, which can give rise to surface productivity and export potential. Atmospheric deposition, a significant factor influencing marine productivity in the South Aegean and Ionian Seas due to the absence of major riverine inputs, introduces substantial amounts of nutrients, trace metals that enhance productivity and particulate fluxes, as well as anthropogenic contaminants [35,89]. During such events, Saharan dust and/or other airborne particles of various origins settle onto the surface waters, contributing both terrestrial and anthropogenic materials to the particle pool [90,91]. This process can increase lithogenic and organic carbon fluxes, as observed in the elevated spring loadings for PC1.

Similar to the seasonality of the South Aegean Sea, PC1 positive loadings are also noted in the Ionian Sea during winter and spring. The peaks in the flux of all biogenic components and associated PAHs during February and March 2015 indicate relatively enhanced productivity in late winter–early spring compared to other seasons. During this period, decreased SST and increased Chl-a values (Figure 2c) resulted from enhanced convective mixing and nutrient upwelling, promoting surface productivity and vertical export fluxes of associated PAH compounds [23,89]. The individual peaks in precipitation rates recorded during this season (Figure 2c) could also be indicative of episodic increases in wet deposition, carrying atmospheric particles that fertilize the sea surface, leading to higher vertical flux value [31,35].

6. Conclusions

This time series data on PAH concentrations and fluxes linked to sinking particles in the NEMS offers valuable insights into their sources, seasonal variations, transport processes, and vertical export to deep basins. Molecular profiles and diagnostic ratios reveal an admixture of pyrolytic, petrogenic, and natural inputs. PMF analysis identifies four key sources—low-temperature combustion (31%), high-temperature combustion (30%), petrogenic inputs (22%), and petrogenic low-MW compounds (17%)—highlighting the dominance of combustion-derived PAHs. PCA emphasizes the central role of marine biogenic particle fluxes, enhanced by atmospheric deposition of elemental carbon, in driving PAH export.

The North Aegean Sea exhibits the highest PAH fluxes, driven by nutrient-rich riverine and Black Sea Water inflows, seasonal productivity patterns, and relatively enhanced anthropogenic inputs. Coccolithophore and siliceous blooms enhance PAH export in late winter and summer, respectively. The Cretan Sea is dominated by inputs from petrogenic sources (~70%), with mesoscale currents redistributing petroleum-related particles. Spring coccolithophore blooms and wet atmospheric deposition contribute to elevated fluxes of POC and petrogenic PAHs to deeper waters. The Ionian Sea exhibits the lowest PAH fluxes, likely influenced by its deep water column depth, which leads to significant PAH degradation due to extended residence times. Atmospheric deposition dominates during periods of low productivity, while the increase in PAHs' export during winter-early spring is related to the seasonal productivity rise, driven by convective mixing and the concomitant nutrient upwelling from the sub-surface layers - and their association to biogenic organic matter which enhance their settling to depth.

Overall, PAH fluxes in the NEMS reflect the complex interplay of pollution sources (e.g., degraded petroleum, unburned fossil fuels, combustion emissions) and transport pathways, including maritime activities, atmospheric deposition, and freshwater inputs. Spatio-temporal variability underscores the determinant role of biogeochemical processes and circulation dynamics in shaping PAH distribution across the region's deep basins.

References

1. Fowler, S.W.; Knauer, G.A. Role of large particles in the transport of elements and organic compounds through the oceanic water column. *Prog. Oceanogr.* **1986**, *16*, 147–194. [CrossRef]
2. Ziveri, P.; Rutten, A.; De Lange, G.J.; Thomson, J.; Corselli, C. Present-day coccolith fluxes recorded in central eastern Mediterranean sediment traps and surface sediments. *Palaeogeogr. Palaeoclimatol. Palaeoecol.* **2000**, *158*, 175–195. [CrossRef]
3. Gogou, A.; Sanchez-Vidal, A.; Durrieu De Madron, X.; Stavrakakis, S.; Calafat, A.M.; Stabholz, M.; Psarra, S.; Canals, M.; Heussner, S.; Stavrakaki, I.; et al. Carbon flux to the deep in three open sites of the Southern European Seas (SES). *J. Mar. Syst.* **2014**, *129*, 224–233. [CrossRef]
4. Bouloubassi, I.; Méjanelle, L.; Pete, R.; Fillaux, J.; Lorre, A.; Point, V. PAH transport by sinking particles in the open Mediterranean Sea: A 1 year sediment trap study. *Mar. Pollut. Bull.* **2006**, *52*, 560–571. [CrossRef] [PubMed]
5. Samanta, S.K.; Singh, O.V.; Jain, R.K. Polycyclic aromatic hydrocarbons: Environmental pollution and bioremediation. *Trends Biotechnol.* **2002**, *20*, 243–248. [CrossRef]
6. EC, 2013. Directive 2013/39/EU of the European Parliament and of the Council of 12 August 2013 Amending Directives 2000/60/EC and 2008/105/EC as Regards Priority Substances in the Field of Water Policy. Available online: https://eur-lex.europa.eu/LexUriServ/LexUriServ.do?uri=OJ:L:2013:226:0001:0017:en:PDF (accessed on 8 November 2024).
7. Latimer, J.S.; Zheng, J. The Sources, Transport, and Fate of PAHs in the Marine Environment. In *PAHs: An Ecotoxicological Perspective*; Douben, P.E.T., Ed.; Wiley: Hoboken, NJ, USA, 2003; pp. 7–33. [CrossRef]
8. Ramdahl, T.; Alfheim, I.; Bjørseth, A. PAH Emission from Various Sources and their Evolution Over the Last Decades. In *Mobile Source Emissions Including Policyclic Organic Species*; Rondia, D., Cooke, M., Haroz, R.K., Eds.; Springer: Dordrecht, The Netherlands, 1983; pp. 277–297. [CrossRef]
9. Yunker, M.B.; Macdonald, R.W. Petroleum biomarker sources in suspended particulate matter and sediments from the Fraser River Basin and Strait of Georgia, Canada. *Org. Geochem.* **2003**, *34*, 1525–1541. [CrossRef]
10. Bouloubassi, I.; Saliot, A. Dissolved, particulate and sedimentary naturally derived polycyclic aromatic hydrocarbons in a coastal environment: Geochemical significance. *Mar. Chem.* **1993**, *42*, 127–143. [CrossRef]

11. Tolosa, I.; Bayona, J.M.; Albaigés, J. Aliphatic and Polycyclic Aromatic Hydrocarbons and Sulfur/Oxygen Derivatives in Northwestern Mediterranean Sediments: Spatial and Temporal Variability, Fluxes, and Budgets. *Environ. Sci. Technol.* **1996**, *30*, 2495–2503. [CrossRef]

12. Farrington, J.; Takada, H. Persistent Organic Pollutants (POPs), Polycyclic Aromatic Hydrocarbons (PAHs), and Plastics: Examples of the Status, Trend, and Cycling of Organic Chemicals of Environmental Concern in the Ocean. *Oceanography* **2014**, *27*, 196–213. [CrossRef]

13. Dachs, J.; Lohmann, R.; Ockenden, W.A.; Méjanelle, L.; Eisenreich, S.J.; Jones, K.C. Oceanic Biogeochemical Controls on Global Dynamics of Persistent Organic Pollutants. *Environ. Sci. Technol.* **2002**, *36*, 4229–4237. [CrossRef]

14. Deyme, R.; Bouloubassi, I.; Taphanel-Valt, M.-H.; Miquel, J.-C.; Lorre, A.; Marty, J.-C.; Méjanelle, L. Vertical fluxes of aromatic and aliphatic hydrocarbons in the Northwestern Mediterranean Sea. *Environ. Pollut.* **2011**, *159*, 3681–3691. [CrossRef]

15. Yunker, M.B.; Macdonald, R.W.; Vingarzan, R.; Mitchell, R.H.; Goyette, D.; Sylvestre, S. PAHs in the Fraser River basin: A critical appraisal of PAH ratios as indicators of PAH source and composition. *Org. Geochem.* **2002**, *33*, 489–515. [CrossRef]

16. Salvadó, J.A.; Grimalt, J.O.; López, J.F.; Palanques, A.; Heussner, S.; Pasqual, C.; Sanchez-Vidal, A.; Canals, M. Transfer of lipid molecules and polycyclic aromatic hydrocarbons to open marine waters by dense water cascading events. *Prog. Oceanogr.* **2017**, *159*, 178–194. [CrossRef]

17. Koudryashova, Y.; Chizhova, T.; Inoue, M.; Hayakawa, K.; Nagao, S.; Marina, E.; Mundo, R. Deep Water PAH Cycling in the Japan Basin (the Sea of Japan). *J. Mar. Sci. Eng.* **2022**, *10*, 2015. [CrossRef]

18. Burns, K.A.; Volkman, J.K.; Cavanagh, J.-A.; Brinkman, D. Lipids as biomarkers for carbon cycling on the Northwest Shelf of Australia: Results from a sediment trap study. *Mar. Chem.* **2003**, *80*, 103–128. [CrossRef]

19. Theodosi, C.; Parinos, C.; Gogou, A.; Kokotos, A.; Stavrakakis, S.; Lykousis, V.; Hatzianestis, J.; Mihalopoulos, N. Downward fluxes of elemental carbon, metals and polycyclic aromatic hydrocarbons in settling particles from the deep Ionian Sea (NESTOR site), Eastern Mediterranean. *Biogeosciences* **2013**, *10*, 4449–4464. [CrossRef]

20. Tsapakis, M.; Apostolaki, M.; Eisenreich, S.; Stephanou, E.G. Atmospheric Deposition and Marine Sedimentation Fluxes of Polycyclic Aromatic Hydrocarbons in the Eastern Mediterranean Basin. *Environ. Sci. Technol.* **2006**, *40*, 4922–4927. [CrossRef]

21. Psarra, S.; Tselepides, A.; Ignatiades, L. Primary productivity in the oligotrophic Cretan Sea (NE Mediterranean): Seasonal and interannual variability. *Prog. Oceanogr.* **2000**, *46*, 187–204. [CrossRef]

22. Bosc, E.; Bricaud, A.; Antoine, D. Seasonal and interannual variability in algal biomass and primary production in the Mediterranean Sea, as derived from 4 years of SeaWiFS observations. *Glob. Biogeochem. Cycles* **2004**, *18*, GB002034. [CrossRef]

23. Stavrakakis, S.; Gogou, A.; Krasakopoulou, E.; Karageorgis, A.P.; Kontoyiannis, H.; Rousakis, G.; Velaoras, D.; Perivoliotis, L.; Kambouri, G.; Stavrakaki, I.; et al. Downward fluxes of sinking particulate matter in the deep Ionian Sea (NESTOR site), eastern Mediterranean: Seasonal and interannual variability. *Biogeosciences* **2013**, *10*, 7235–7254. [CrossRef]

24. Lipizer, M.; Berto, D.; Cermelj, B.; Fafandjel, M.; Formalewicz, M.; Hatzianestis, I.; Ilijanić, N.; Kaberi, H.; Kralj, M.; Matijevic, S.; et al. Trace metals and polycyclic aromatic hydrocarbons in the Eastern Mediterranean sediments: Concentration ranges as a tool for quality control of large data collections. *Mar. Pollut. Bull.* **2022**, *185*, 114181. [CrossRef] [PubMed]

25. Ivanova, M. UNEP in Global Environmental Governance: Design, Leadership, Location. *Glob. Environ. Politics* **2010**, *10*, 30–59. [CrossRef]

26. Parinos, C.; Gogou, A.; Bouloubassi, I.; Stavrakakis, S.; Plakidi, E.; Hatzianestis, I. Sources and downward fluxes of polycyclic aromatic hydrocarbons in the open southwestern Black Sea. *Org. Geochem.* **2013**, *57*, 65–75. [CrossRef]

27. Lelieveld, J.; Berresheim, H.; Borrmann, S.; Crutzen, P.J.; Dentener, F.J.; Fischer, H.; Feichter, J.; Flatau, P.J.; Heland, J.; Holzinger, R.; et al. Global Air Pollution Crossroads over the Mediterranean. *Science* **2002**, *298*, 794–799. [CrossRef] [PubMed]

28. Kanakidou, M.; Duce, R.A.; Prospero, J.M.; Baker, A.R.; Benitez-Nelson, C.; Dentener, F.J.; Hunter, K.A.; Liss, P.S.; Mahowald, N.; Okin, G.S.; et al. Atmospheric fluxes of organic N and P to the global ocean. *Glob. Biogeochem. Cycles* **2012**, *26*, 2011GB004277. [CrossRef]

29. Zervakis, V.; Georgopoulos, D.; Karageorgis, A.P.; Theocharis, A. On the response of the Aegean Sea to climatic variability: A review. *Int. J. Climatol.* **2004**, *24*, 1845–1858. [CrossRef]

30. Krasakopoulou, E.; Zervakis, V.; Souvermezoglou, E.; Georgopoulos, D. North-eastern Aegean sea: An effort to estimate steady-state N & P budgets during September 1998. *Mediterr. Mar. Sci.* **2002**, *3*, 43–54. [CrossRef]

31. Nikolopoulou, I.; Skampa, E.; Varkitzi, I.; Dimiza, M.D.; Parinos, C.; Kambouri, G.; Stavrakaki, I.; Gogou, A.; Triantaphyllou, M.V. The Contribution of Siliceous Plankton to Vertical Export Flux in the Eastern Mediterranean: A Comparative Study of the North Aegean, Cretan, and Ionian Seas. *J. Mar. Sci. Eng.* **2024**, *12*, 2084. [CrossRef]

32. Tsiaras, K.P.; Petihakis, G.; Kourafalou, V.H.; Triantafyllou, G. Impact of the river nutrient load variability on the North Aegean ecosystem functioning over the last decades. *J. Sea Res.* **2014**, *86*, 97–109. [CrossRef]

33. Jarosz, E.; Teague, W.J.; Book, J.W.; Beşiktepe, Ş.T. Observed volume fluxes and mixing in the Dardanelles Strait. *J. Geophys. Res. Ocean.* **2013**, *118*, 5007–5021. [CrossRef]

34. Poulos, S.E.; Drakopoulos, P.G.; Collins, M.B. Seasonal variability in sea surface oceanographic conditions in the Aegean Sea (Eastern Mediterranean): An overview. *J. Mar. Syst.* **1997**, *13*, 225–244. [CrossRef]

35. Skampa, E.; Triantaphyllou, M.V.; Dimiza, M.D.; Gogou, A.; Malinverno, E.; Stavrakakis, S.; Parinos, C.; Panagiotopoulos, I.; Tselenti, D.; Archontikis, O.; et al. Coccolithophore export in three deep-sea sites of the Aegean and Ionian Seas (Eastern Mediterranean): Biogeographical patterns and biogenic carbonate fluxes. *Deep Sea Res. Part II Top. Stud. Oceanogr.* **2020**, *171*, 104690. [CrossRef]

36. Velaoras, D.; Krokos, G.; Nittis, K.; Theocharis, A. Dense intermediate water outflow from the C retan S ea: A salinity driven, recurrent phenomenon, connected to thermohaline circulation changes. *J. Geophys. Res. Ocean.* **2014**, *119*, 4797–4820. [CrossRef]

37. Civitarese, G.; Gačić, M.; Lipizer, M.; Eusebi Borzelli, G.L. On the impact of the Bimodal Oscillating System (BiOS) on the biogeochemistry and biology of the Adriatic and Ionian Seas (Eastern Mediterranean). *Biogeosciences* **2010**, *7*, 3987–3997. [CrossRef]

38. Larnicol, G.; Ayoub, N.; Le Traon, P.Y. Major changes in Mediterranean Sea level variability from 7 years of TOPEX/Poseidon and ERS-1/2 data. *J. Mar. Syst.* **2002**, *33–34*, 63–89. [CrossRef]

39. Malanotte-Rizzoli, P.; Manca, B.B.; Ribera D'Alcalà, M.; Theocharis, A.; Bergamasco, A.; Bregant, D.; Budillon, G.; Civitarese, G.; Georgopoulos, D.; Michelato, A.; et al. A synthesis of the Ionian Sea hydrography, circulation and water mass pathways during POEM-Phase I. *Prog. Oceanogr.* **1997**, *39*, 153–204. [CrossRef]

40. Nittis, K.; Lascaratos, A.; Theocharis, A. Dense water formation in the Aegean Sea: Numerical simulations during the Eastern Mediterranean Transient. *J. Geophys. Res. Ocean.* **2003**, *108*, 8120. [CrossRef]

41. Theocharis, A.; Balopoulos, E.; Kioroglou, S.; Kontoyiannis, H.; Iona, A. A synthesis of the circulation and hydrography of the South Aegean Sea and the Straits of the Cretan Arc (March 1994–January 1995). *Prog. Oceanogr.* **1999**, *44*, 469–509. [CrossRef]

42. Heussner, S.; Ratti, C.; Carbonne, J. The PPS 3 time-series sediment trap and the trap sample processing techniques used during the ECOMARGE experiment. *Cont. Shelf Res.* **1990**, *10*, 943–958. [CrossRef]

43. Gogou, A.I.; Apostolaki, M.; Stephanou, E.G. Determination of organic molecular markers in marine aerosols and sediments: One-step flash chromatography compound class fractionation and capillary gas chromatographic analysis. *J. Chromatogr. A* **1998**, *799*, 215–231. [CrossRef]

44. Heussner, S.; Durrieu De Madron, X.; Calafat, A.; Canals, M.; Carbonne, J.; Delsaut, N.; Saragoni, G. Spatial and temporal variability of downward particle fluxes on a continental slope: Lessons from an 8-yr experiment in the Gulf of Lions (NW Mediterranean). *Mar. Geol.* **2006**, *234*, 63–92. [CrossRef]

45. Nieuwenhuize, J.; Maas, Y.E.M.; Middelburg, J.J. Rapid analysis of organic carbon and nitrogen in particulate materials. *Mar. Chem.* **1994**, *45*, 217–224. [CrossRef]

46. Birch, M.E.; Cary, R.A. Elemental Carbon-Based Method for Monitoring Occupational Exposures to Particulate Diesel Exhaust. *Aerosol Sci. Technol.* **1996**, *25*, 221–241. [CrossRef]

47. Theodosi, C.; Markaki, Z.; Tselepides, A.; Mihalopoulos, N. The significance of atmospheric inputs of soluble and particulate major and trace metals to the eastern Mediterranean seawater. *Mar. Chem.* **2010**, *120*, 154–163. [CrossRef]

48. Mandić, J.; Veža, J.; Kušpilić, G. Application of Positive Matrix Factorization for Source Apportionment of Polycyclic Aromatic Hydrocarbons (PAH) in the Adriatic Sea, and the Evaluation of PAH-Related Carcinogenic Risks. *Appl. Sci.* **2023**, *13*, 6992. [CrossRef]

49. Saba, T. Using positive matrix factorization to unmix PAH fingerprints in contaminated sediments. *Environ. Monit. Assess.* **2023**, *195*, 1003. [CrossRef]

50. Meglen, R.R. Examining large databases: A chemometric approach using principal component analysis. *J. Chemom.* **1991**, *5*, 163–179. [CrossRef]

51. Pedrosa-Pàmies, R.; Parinos, C.; Sanchez-Vidal, A.; Gogou, A.; Calafat, A.; Canals, M.; Bouloubassi, I.; Lampadariou, N. Composition and sources of sedimentary organic matter in the deep eastern Mediterranean Sea. *Biogeosciences* **2015**, *12*, 7379–7402. [CrossRef]

52. Parinos, C.; Skylaki, E.; Hatzianestis, I.; Gogou, A. Occurrence, sources and water column distribution trends of suspended particle-associated aliphatic and polycyclic aromatic hydrocarbons in the open northeastern Mediterranean Sea. *Sci. Total Environ.* **2024**, *914*, 169685. [CrossRef]

53. Eglinton, G.; Hamilton, R.J. Leaf Epicuticular Waxes. *Science* **1967**, *80*, 1322–1335. [CrossRef]

54. Collister, J.W.; Lichtfouse, E.; Hieshima, G.; Hayes, J.M. Partial resolution of sources of n-alkanes in the saline portion of the Parachute Creek Member, Green River Formation (Piceance Creek Basin, Colorado). *Org. Geochem.* **1994**, *21*, 645–659. [CrossRef] [PubMed]

55. Wang, Z.; Fingas, M.; Page, D.S. Oil spill identification. *J. Chromatogr. A* **1999**, *843*, 369–411. [CrossRef]

56. Yunker, M.B.; Belicka, L.L.; Harvey, H.R.; Macdonald, R.W. Tracing the inputs and fate of marine and terrigenous organic matter in Arctic Ocean sediments: A multivariate analysis of lipid biomarkers. *Deep Sea Res. Part II Top. Stud. Oceanogr.* **2005**, *52*, 3478–3508. [CrossRef]

57. Neff, J.M.; Stout, S.A.; Gunster, D.G. Ecological risk assessment of polycyclic aromatic hydrocarbons in sediments: Identifying sources and ecological hazard. *Integr. Environ. Assess. Manag.* **2005**, *1*, 22–33. [CrossRef]

58. Dachs, J.; Bayona, J.M.; Fowler, S.W.; Miquel, J.-C.; Albaigés, J. Vertical fluxes of polycyclic aromatic hydrocarbons and organochlorine compounds in the western Alboran Sea (southwestern Mediterranean). *Mar. Chem.* **1996**, *52*, 75–86. [CrossRef]

59. Lipiatou, E.; Marty, J.-C.; Saliot, A. Sediment trap fluxes of polycyclic aromatic hydrocarbons in the Mediterranean Sea. *Mar. Chem.* **1993**, *44*, 43–54. [CrossRef]

60. Raoux, C.; Boyona, J.M.; Miquel, J.-C.; Teyssie, J.-L.; Fowler, S.W.; Albaigés, J. Particulate Fluxes of Aliphatic and Aromatic Hydrocarbons in Near-shore Waters to the Northwestern Mediterranean Sea, and the Effect of Continental Runoff. *Estuar. Coast. Shelf Sci.* **1999**, *48*, 605–616. [CrossRef]

61. Bates, T.S.; Hamilton, S.E.; Cline, J.D. Vertical transport and sedimentation of hydrocarbons in the central main basin of Puget Sound, Washington [USA]. *Environ. Sci. Technol.* **1984**, *18*, 299–305. [CrossRef] [PubMed]

62. Broman, D.; Colmsjoe, A.; Ganning, B.; Naef, C.; Zebuhr, Y. A multi-sediment trap study on the temporal and spatial variability of polycyclic aromatic hydrocarbons and lead in an anthropogenic influenced archipelago. *Environ. Sci. Technol.* **1988**, *22*, 1219–1228. [CrossRef] [PubMed]

63. Takada, H.; Farrington, J.W.; Bothner, M.H.; Johnson, C.G.; Tripp, B.W. Transport of Sludge-Derived Organic Pollutants to Deep-Sea Sediments at Deep Water Dump Site 106. *Environ. Sci. Technol.* **1994**, *28*, 1062–1072. [CrossRef]

64. Palm, A.; Cousins, I.; Gustafsson, Ö.; Axelman, J.; Grunder, K.; Broman, D.; Brorström-Lundén, E. Evaluation of sequentially-coupled POP fluxes estimated from simultaneous measurements in multiple compartments of an air–water–sediment system. *Environ. Pollut.* **2004**, *128*, 85–97. [CrossRef] [PubMed]

65. Fang, M.-D.; Chang, W.-K.; Lee, C.-L.; Liu, J.T. The use of polycyclic aromatic hydrocarbons as a particulate tracer in the water column of Gaoping (Kaoping) Submarine Canyon. *J. Mar. Syst.* **2009**, *76*, 457–467. [CrossRef]

66. Adhikari, P.L.; Maiti, K.; Overton, E.B. Vertical fluxes of polycyclic aromatic hydrocarbons in the northern Gulf of Mexico. *Mar. Chem.* **2015**, *168*, 60–68. [CrossRef]

67. Laughlin, R.B.; Neff, J.M. Interactive effects of salinity, temperature and polycyclic aromatic hydrocarbons on the survival and development rate of larvae of the mud crabRhithropanopeus harrisii. *Mar. Biol.* **1979**, *53*, 281–291. [CrossRef]

68. Wakeham, S.G.; Schaffner, C.; Giger, W. Polycyclic aromatic hydrocarbons in recent lake sediments—II. Compounds derived from biogenic precursors during early diagenesis. *Geochim. Et Cosmochim. Acta* **1980**, *44*, 415–429. [CrossRef]

69. Sporstol, S.; Gjos, N.; Lichtenthaler, R.G.; Gustavsen, K.O.; Urdal, K.; Oreld, F.; Skei, J. Source identification of aromatic hydrocarbons in sediments using GC/MS. *Environ. Sci. Technol.* **1983**, *17*, 282–286. [CrossRef]

70. Yunker, M.B.; Macdonald, R.W.; Snowdon, L.R.; Fowler, B.R. Alkane and PAH biomarkers as tracers of terrigenous organic carbon in Arctic Ocean sediments. *Org. Geochem.* **2011**, *42*, 1109–1146. [CrossRef]

71. Sun, X.; Wang, H.; Guo, Z.; Lu, P.; Song, F.; Liu, L.; Liu, J.; Rose, N.L.; Wang, F. Positive matrix factorization on source apportionment for typical pollutants in different environmental media: A review. *Environ. Sci. Process. Impacts* **2020**, *22*, 239–255. [CrossRef] [PubMed]

72. Yuan, Z.; He, B.; Wu, X.; Simonich SL, M.; Liu, H.; Fu, J.; Chen, A.; Liu, H.; Wang, Q. Polycyclic aromatic hydrocarbons (PAHs) in urban stream sediments of Suzhou Industrial Park, an emerging eco-industrial park in China: Occurrence, sources and potential risk. *Ecotoxicol. Environ. Saf.* **2021**, *214*, 112095. [CrossRef] [PubMed]

73. Hatzianestis, I.; Parinos, C.; Chourdaki, S.; Plakidi, E.; Abualnaja, Y.; Hoteit, I.; Churchill, J.; Papageorgiou, D.; Papadopoulos, V.; Alshehri, Y.; et al. Organic contaminants levels, distribution and risk assessment in Jeddah marine coastal zone sediments. *Mar. Pollut. Bull.* **2024**, *199*, 115926. [CrossRef]

74. Fine, P.M.; Cass, G.R.; Simoneit, B.R.T. Chemical Characterization of Fine Particle Emissions from Fireplace Combustion of Woods Grown in the Northeastern United States. *Environ. Sci. Technol.* **2001**, *35*, 2665–2675. [CrossRef] [PubMed]

75. Ferraro, G.; Baschek, B.; De Montpellier, G.; Njoten, O.; Perkovic, M.; Vespe, M. On the SAR derived alert in the detection of oil spills according to the analysis of the EGEMP. *Mar. Pollut. Bull.* **2010**, *60*, 91–102. [CrossRef] [PubMed]

76. Carpenter, A.; Kostianoy, A.G. (Eds.) Oil Pollution in the Mediterranean Sea: Part I: The International Context. In *The Handbook of Environmental Chemistry*; Springer International Publishing: Cham, Switzerland, 2018; p. 83. [CrossRef]

77. Castro-Jiménez, J.; Berrojalbiz, N.; Wollgast, J.; Dachs, J. Polycyclic aromatic hydrocarbons (PAHs) in the Mediterranean Sea: Atmospheric occurrence, deposition and decoupling with settling fluxes in the water column. *Environ. Pollut.* **2012**, *166*, 40–47. [CrossRef] [PubMed]

78. Tsapakis, M.; Stephanou, E.G. Polycyclic Aromatic Hydrocarbons in the Atmosphere of the Eastern Mediterranean. *Environ. Sci. Technol.* **2005**, *39*, 6584–6590. [CrossRef] [PubMed]

79. Tsiodra, I.; Grivas, G.; Tavernaraki, K.; Bougiatioti, A.; Apostolaki, M.; Paraskevopoulou, D.; Gogou, A.; Parinos, C.; Oikonomou, K.; Tsagkaraki, M.; et al. Annual exposure to polycyclic aromatic hydrocarbons in urban environments linked to wintertime wood-burning episodes. *Atmos. Chem. Phys.* **2021**, *21*, 17865–17883. [CrossRef]

80. Tsiodra, I.; Grivas, G.; Bougiatioti, A.; Tavernaraki, K.; Parinos, C.; Paraskevopoulou, D.; Papoutsidaki, K.; Tsagkaraki, M.; Kozonaki, F.-A.; Oikonomou, K.; et al. Source apportionment of particle-bound polycyclic aromatic hydrocarbons (PAHs), oxygenated PAHs (OPAHs), and their associated long-term health risks in a major European city. *Sci. Total Environ.* **2024**, *951*, 175416. [CrossRef] [PubMed]

81. Krom, M.D.; Kress, N.; Brenner, S.; Gordon, L.I. Phosphorus limitation of primary productivity in the eastern Mediterranean Sea. *Limnol. Oceanogr.* **1991**, *36*, 424–432. [CrossRef]

82. Pavlidou, A.; Velaoras, D.; Karageorgis, A.P.; Rousselaki, E.; Parinos, C.; Dähnke, K.; Möbius, J.; Meador, T.; Psarra, S.; Frangoulis, C.; et al. Seasonal variations of biochemical and optical properties, physical dynamics and N stable isotopic composition in three northeastern Mediterranean basins (Aegean, Cretan and Ionian Seas). *Deep Sea Res. Part II Top. Stud. Oceanogr.* **2020**, *171*, 104704. [CrossRef]

83. Berrojalbiz, N.; Lacorte, S.; Calbet, A.; Saiz, E.; Barata, C.; Dachs, J. Accumulation and Cycling of Polycyclic Aromatic Hydrocarbons in Zooplankton. *Environ. Sci. Technol.* **2009**, *43*, 2295–2301. [CrossRef] [PubMed]

84. Dachs, J.; Eisenreich, S.J. Adsorption onto Aerosol Soot Carbon Dominates Gas-Particle Partitioning of Polycyclic Aromatic Hydrocarbons. *Environ. Sci. Technol.* **2000**, *34*, 3690–3697. [CrossRef]

85. Gustafsson, Ö.; Gschwend, P.M.; Buesseler, K.O. Using 234Th disequilibria to estimate the vertical removal rates of polycyclic aromatic hydrocarbons from the surface ocean. *Mar. Chem.* **1997**, *57*, 11–23. [CrossRef]

86. Meyers, P.A. Organic geochemical proxies of paleoceanographic, paleolimnologic, and paleoclimatic processes. *Org. Geochem.* **1997**, *27*, 213–250. [CrossRef]

87. Zervakis, V.; Georgopoulos, D.; Drakopoulos, P.G. The role of the North Aegean in triggering the recent Eastern Mediterranean climatic changes. *J. Geophys. Res. Ocean.* **2000**, *105*, 26103–26116. [CrossRef]

88. Mamoutos, I.G.; Potiris, E.; Androulidakis, Y.; Tragou, E.; Zervakis, V. Evidence for Reduced Black Sea Water Outflow to the North Aegean. *Earth Space Sci.* **2024**, *11*, e2024EA003674. [CrossRef]

89. Boyd, P.W.; Strzepek, R.; Fu, F.; Hutchins, D.A. Environmental control of open-ocean phytoplankton groups: Now and in the future. *Limnol. Oceanogr.* **2010**, *55*, 1353–1376. [CrossRef]

90. Malinverno, E.; Cerino, F.; Karatsolis, B.T.; Ravani, A.; Dimiza, M.; Psarra, S.; Gogou, A.; Triantaphyllou, M.V. Silicoflagellates in the eastern mediterranean and Black Seas: Seasonality, distribution and sedimentary record. *Deep Sea Res. Part II Top. Stud. Oceanogr.* **2019**, *164*, 122–134. [CrossRef]

91. Jickells, T.D.; An, Z.S.; Andersen, K.K.; Baker, A.R.; Bergametti, G.; Brooks, N.; Cao, J.J.; Boyd, P.W.; Duce, R.A.; Hunter, K.A.; et al. Global Iron Connections Between Desert Dust, Ocean Biogeochemistry, and Climate. *Science* **2005**, *308*, 67–71. [CrossRef]